Isospin-breaking effects of the double-charm molecular pentaquarks

Fei-Yu Chen,[1] Ning Li,[1,*] and Wei Chen[1,2,†]

[1]*School of Physics, Sun Yat-Sen University, Guangzhou 510275, China*

[2]*Southern Center for Nuclear-Science Theory (SCNT), Institute of Modern Physics, Chinese Academy of Sciences, Huizhou 516000, Guangdong Province, China*

(Received 25 March 2026; accepted 15 June 2026; published 13 July 2026)

We investigate isospin-breaking effects in double-charm molecular pentaquarks with the $D^{(*)}\Sigma_c^{(*)}$ configuration, using the one-boson-exchange potential framework. In these systems, the isospin-breaking effects arise from two sources: the strong interaction, which manifests as the threshold difference of the $D^{(*)}\Sigma_c^{(*)}$ components in the same isospin multiplet and the mass splittings of the exchanged isovector mesons (π and ρ), and the electromagnetic interaction between charged $D^{(*)}$ and $\Sigma_c^{(*)}$ components. We calculate the binding properties and the isospin mixing angle between the $I = 1/2$ and $I = 3/2$ states of the $D^{(*)}\Sigma_c^{(*)}$ system. Our results show that the isospin-breaking effect contributes a significant correction of roughly 10%–30% to the binding energy. This effect is particularly pronounced in loosely bound molecular candidates, which are characterized by small binding energies and large root-mean-square radii. We therefore conclude that the explicit inclusion of isospin-breaking effects is essential for achieving the precision in theoretical calculations necessary to match rapidly advancing experimental programs. Our results are expected to provide valuable guidance for future high-precision experimental studies of deuteronlike molecular states.

DOI: 10.1103/ssh8-5fbr

I. INTRODUCTION

The observation of the $X(3872)$ by the Belle Collaboration in 2003 [1] marked the beginning of a remarkable era, triggering a plethora of discoveries of unexpected hadron states over the following two decades. These new hadron states challenge the conventional quark model, including the charged charmoniumlike $Z_c(3900)$ [2,3], the hidden-charm pentaquark family $P_\psi(4312)$, $P_\psi(4440)$, $P_\psi(4457)$, $P_{\psi s}(4459)$, $P^{\Lambda}_{\psi s}(4338)$ [4–7], the doubly charmed tetraquark state $T^{+}_{cc}(3875)$ [8], etc., which are considered as candidates of exotic hadron states. Collectively, these discoveries have reshaped our understanding of hadron spectroscopy, and for comprehensive overviews of the experimental and theoretical progress on these exotic states, we refer the reader to recent review articles [9–19].

The experimental discoveries have prompted intensive theoretical investigations into the nature of these states, giving rise to numerous configurational interpretations, such as glueballs, hybrids, compact multiquarks, and hadronic molecules. The hadronic molecule interpretation holds particular interest for two key reasons. The first is the well-established precedent of the deuteron itself, a proton-neutron bound state, which proves that color-singlet hadrons can be exchanged to form molecular systems. The second is the observation that many of the newly observed states lie remarkably close to the thresholds of two conventional hadrons, a characteristic feature expected for loosely bound molecular states composed of color-singlet constituents. A schematic comparison of the compact multiquark and hadronic molecule configurations is shown in Fig. 1.

The rapid progress in experimental studies of exotic hadrons has brought hidden-charm tetraquarks and pentaquarks to the forefront of hadronic physics. In fact, theoretical predictions of hidden-charm pentaquarks with the $\bar{D}^{(*)}\Sigma_c^{(*)}$ molecular configuration were already made more than a decade ago [20–25]. After the observation of the P_ψ states in 2015 [4], numerous theoretical studies further explored their molecular pentaquark interpretations [26–30]. As the doubly charmed counterpart to the hidden-charm pentaquarks, the double-charm pentaquark P_{cc} was investigated using one-boson-exchange (OBE) model since 2010s [31–34]. More recently, predictions for double-charm pentaquark states have proliferated across various theoretical frameworks, including using the QCD sum rules [35–40],

*Contact author: lining59@mail.sysu.edu.cn

†Contact author: chenwei29@mail.sysu.edu.cn

Published by the American Physical Society under the terms of the Creative Commons Attribution 4.0 International license. Further distribution of this work must maintain attribution to the author(s) and the published article's title, journal citation, and DOI. Funded by SCOAP³.

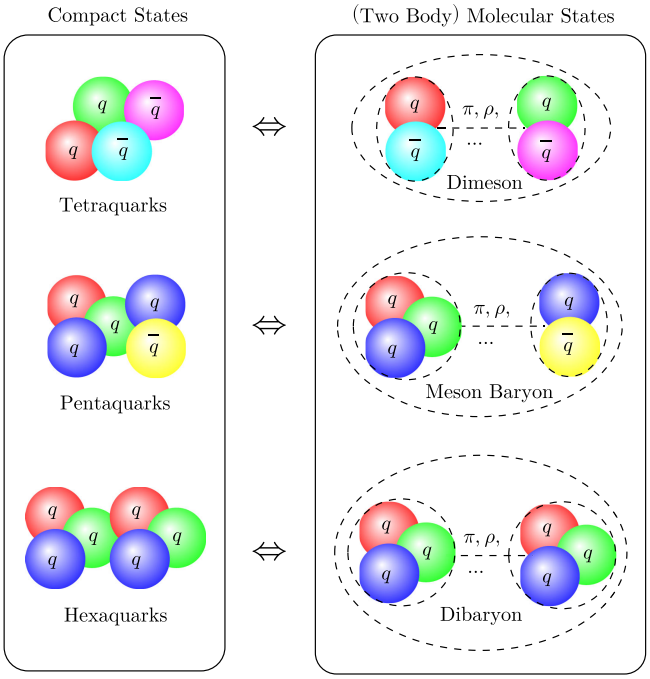


FIG. 1. A schematic picture of the multiquark states, compact multiquarks (left panel) versus hadronic molecules (right panel) formed by the colorless hadrons.

the chiral effective field theory [41–43], the (chiral) quark model [44–48], the quark delocalization color screening model method [49], the unitarized coupled-channel approach [50], and so on.

As experimental datasets continue to grow in both size and precision, high-quality theoretical calculations are urgently needed to keep pace. Approximations commonly employed in phenomenological studies, such as perfect isospin symmetry, are no longer sufficient to meet the demands of future experimental investigations. Indeed, several recent studies have highlighted the importance of incorporating electromagnetic contributions in hadronic systems. For instance, lattice QCD and OBE model analyses of the $\Omega_{ccc}\Omega_{ccc}$ dibaryon show that while the system is bound by several MeV through residual strong interactions alone, it becomes unbound once electromagnetic effects are included [51,52]. In contrast, the $\Omega_{bbb}\Omega_{bbb}$ dibaryon remains deeply bound even with electromagnetic interaction, exhibiting a binding energy up to 89 MeV, with Coulomb corrections playing only a minor role [53]. As for the extensively studied $X(3872)$, isospin-breaking effects modify its binding energy by less than 1 MeV, yet they prove essential for correctly describing its decay patterns [54,55]. These examples underscore the importance of accounting for isospin-breaking effects when striving for the precision required by contemporary and forthcoming experiments.

In the present work, we investigate isospin-breaking effects in double-charm hadronic molecules composed of a charmed meson $D^{(*)}$ and a charmed baryon $\Sigma_c^{(*)}$, within the framework of OBE model. To manifest the isospin-breaking effect, we omit coupled-channel effects between distinct flavor channels. However, we do include the mixing between different partial waves induced by the tensor force, which couples orbital angular momentum states differing by $\Delta l = 2$.

The paper is organized as follows. After the introduction of Sec. I, we describe the theoretical framework including the spin-isospin wave functions, the strong forces, Coulomb forces, and the Schrödinger equation with isospin breaking in Sec. II. Our numerical results and their analyses are presented in Sec. III. The last section is a brief summary and discussion. Detailed notations and formulas used throughout the paper are provided in the Appendix.

II. THEORETICAL FRAMEWORK

In this section, we will present the theoretical formalism. We first give the spin and isospin wave functions for the $D^{(*)}\Sigma_c^{(*)}$ systems. Then we derive the strong interaction between a charmed meson $D^{(*)}$ and a charmed baryon $\Sigma_c^{(*)}$, which is accounted by exchanging a light meson (such as π, ρ, σ, etc.) within the one-boson-exchange potential model. After that, we discuss the isospin breaking in detail. Lastly, we present the matrix of the Schrödinger equation with isospin breaking.

A. Spin and isospin wave functions

To give prominence to the isospin-breaking effects, we do not consider the coupled-channel effects in the flavor space, but the mixing between different partial waves. Thus, there are four systems for $D^{(*)}\Sigma_c^{(*)}$ in the flavor space, $D\Sigma_c$, $D\Sigma_c^*$, $D^*\Sigma_c$, and $D^*\Sigma_c^*$, which are marked as 11, 22, 33, and 44, respectively, as shown in Fig. 2 for the Feynman diagrams at tree level.

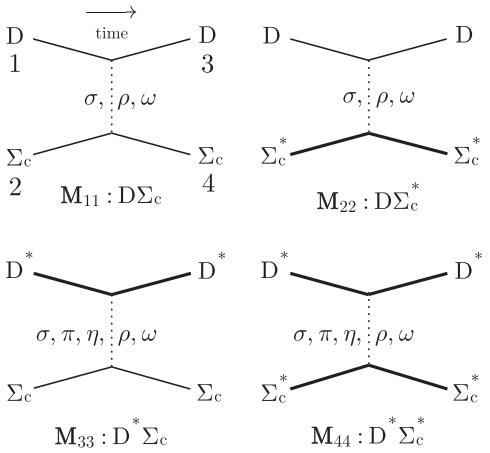


FIG. 2. Tree-level Feynman diagrams for the four scattering processes $D^{(*)}\Sigma_c^{(*)} \to D^{(*)}\Sigma_c^{(*)}$.

TABLE I. The partial waves, denoted by the spectroscopic notation $^{2S+1}L_J$, for each spin-parity state are considered. We truncate the partial-wave expansion at the D-wave ($l = 2$), as the contribution from higher partial waves is expected to be negligible.

J^P	$D\Sigma_c$	$D\Sigma_c^*$	$D^*\Sigma_c$	$D^*\Sigma_c^*$
$\frac{1}{2}^-$	$\vert^2S_{1/2}\rangle$	×	$\begin{pmatrix}\vert^2S_{1/2}\rangle\\ \vert^4D_{1/2}\rangle\end{pmatrix}$	$\begin{pmatrix}\vert^2S_{1/2}\rangle\\ \vert^4D_{1/2}\rangle\\ \vert^6D_{1/2}\rangle\end{pmatrix}$
$\frac{3}{2}^-$	×	$\begin{pmatrix}\vert^4S_{3/2}\rangle\\ \vert^4D_{3/2}\rangle\end{pmatrix}$	$\begin{pmatrix}\vert^4S_{3/2}\rangle\\ \vert^2D_{3/2}\rangle\\ \vert^4D_{3/2}\rangle\end{pmatrix}$	$\begin{pmatrix}\vert^4S_{3/2}\rangle\\ \vert^2D_{3/2}\rangle\\ \vert^4D_{3/2}\rangle\\ \vert^6D_{3/2}\rangle\end{pmatrix}$
$\frac{5}{2}^-$	×	×	×	$\begin{pmatrix}\vert^6S_{5/2}\rangle\\ \vert^2D_{5/2}\rangle\\ \vert^4D_{5/2}\rangle\\ \vert^6D_{5/2}\rangle\end{pmatrix}$

For each $D^{(*)}\Sigma_c^{(*)}$ system, we consider both the ground state (S-wave) configuration and its mixing with higher partial waves. Specifically, we investigate the following spin-parity assignments: $J^P = 1/2^-$ for $D\Sigma_c$; $J^P = 3/2^-$ for $D\Sigma_c^*$; $J^P = 1/2^-, 3/2^-$ for $D^*\Sigma_c$; and $J^P = 1/2^-, 3/2^-, 5/2^-$ for $D^*\Sigma_c^*$. The partial-wave compositions considered for each spin-parity state are summarized in Table I.

The nonvanishing off-diagonal matrix elements of the tensor interaction (see Appendix B for details) cause mixing between partial waves with orbital angular momenta l and $l \pm 2$. In the present study, we incorporate both S-wave and D-wave components. We define P_i as the probability of the ith channel in the state $^{2S+1}L_J$. The total wave function can be expressed as

$$|\Psi\rangle = \sum_i R_i(r)|^{2S+1}L_J\rangle_i, \tag{1}$$

where $R_i(r)$ represents the radial wave function of the ith channel. The probability of each partial-wave component is evaluated from the normalized wave function via the integral

$$P_i = \int |R_i(r)|^2 r^2 dr. \tag{2}$$

Under isospin symmetry, the total isospin of $D^{(*)}\Sigma_c^{(*)}$ could be $I = 1/2$ or $3/2$. In the isospin-1/2 case, there are two degenerate states, $|1/2, \pm 1/2\rangle$, while the isospin-3/2 case yields four degenerate states, $|3/2, \pm 3/2\rangle$ and $|3/2, \pm 1/2\rangle$. However, once the specific isospin breaking is considered, the degeneration is dissolved. In the following, we present the explicit isospin wave functions for the $D\Sigma_c$ system. For isospin-3/2,

$$\begin{aligned}
|3/2, 3/2\rangle &= |D^+\Sigma_c^{++}\rangle,\\
|3/2, 1/2\rangle &= \sqrt{\frac{2}{3}}|D^+\Sigma_c^+\rangle - \sqrt{\frac{1}{3}}|D^0\Sigma_c^{++}\rangle,\\
|3/2, -1/2\rangle &= \sqrt{\frac{1}{3}}|D^+\Sigma_c^0\rangle - \sqrt{\frac{2}{3}}|D^0\Sigma_c^+\rangle,\\
|3/2, -3/2\rangle &= -|D^0\Sigma_c^0\rangle,
\end{aligned} \tag{3}$$

while for isospin-1/2

$$\begin{aligned}
|1/2, 1/2\rangle &= \sqrt{\frac{1}{3}}|D^+\Sigma_c^+\rangle + \sqrt{\frac{2}{3}}|D^0\Sigma_c^{++}\rangle,\\
|1/2, -1/2\rangle &= \sqrt{\frac{2}{3}}|D^+\Sigma_c^0\rangle + \sqrt{\frac{1}{3}}|D^0\Sigma_c^+\rangle.
\end{aligned} \tag{4}$$

The isospin wave functions for other $D^{(*)}\Sigma_c^{(*)}$ systems are similar. From Eqs. (3)–(4), it is evident that the Coulomb force contributes only to the charged isospin configurations, specifically the $|3/2, 3/2\rangle$, $|3/2, 1/2\rangle$, and $|1/2, 1/2\rangle$ states. The remaining states are neutral and thus receive no Coulomb contribution, as they involve either a D^0 or Σ_c^0.

B. The effective strong interaction

We derive the strong interaction between a charmed $D^{(*)}$ and a charmed $\Sigma_c^{(*)}$ within the OBE potential model. We start from the Lagrangians satisfying the heavy quark symmetry and light SU(3)-flavor symmetry [56–61],

$$\mathscr{L}_{\rm eff} = \mathscr{L}_{\mathbb{M}} + \mathscr{L}_{\mathbb{B}}, \tag{5}$$

in which $\mathscr{L}_{\mathbb{M}}$ is for the mesonic part while $\mathscr{L}_{\mathbb{B}}$ is for the baryonic part. Specifically,

$$\begin{aligned}
\mathscr{L}_{\mathbb{M}} = {} & g_{\rm S}\langle H_m \sigma \bar{H}_m\rangle + {\rm i}\beta\langle H_n v_\rho (V^\rho - \mathbb{V}'^\rho)_{nm}\bar{H}_m\rangle\\
& + {\rm i}g\langle H_n X^\rho_{nm}\gamma_\rho\gamma_5\bar{H}_m\rangle + {\rm i}\lambda\langle H_n F^{\alpha\beta}_{nm}\sigma_{\alpha\beta}\bar{H}_m\rangle,
\end{aligned} \tag{6}$$

and

$$\begin{aligned}
\mathscr{L}_{\mathbb{B}} = {} & l_{\rm S} g_{\mu\nu}{\rm Tr}[\bar{S}^\mu \sigma S^\nu] + {\rm i}\beta_{\rm S} g_{\mu\nu}{\rm Tr}[\bar{S}^\mu (V^\rho - \mathbb{V}'^\rho) v_\rho S^\nu]\\
& + \frac{3}{2} g_1 \varepsilon_{\mu\nu\alpha\beta} v^\beta {\rm Tr}[\bar{S}^\mu X^\alpha S^\nu] + \lambda_{\rm S}{\rm Tr}[\bar{S}^\mu F_{\mu\nu} S^\nu],
\end{aligned} \tag{7}$$

where H is a superfield formed by the heavy pseudoscalar and vector mesons under the heavy quark spin symmetry (HQSS). The specific expression of H is

$$H_a \equiv \frac{1+\not{v}}{2}(\gamma_\mu P_a^{*\mu} - \gamma_5 P_a), \tag{8}$$

while the conjugate field $\bar{H}$ is defined as

$$\bar{H}_a \equiv \gamma^0 H_a^\dagger \gamma^0 = (\gamma_\mu P_a^{*\mu\dagger} + \gamma_5 P_a^\dagger)\frac{1+\not{v}}{2}. \tag{9}$$

Here,

$$P^{(*)} = (D^{(*)0}, D^{(*)+}, D_s^{(*)})^{\mathrm{T}} \tag{10}$$

is the vector formed by the heavy pseudoscalar (vector) mesons under the light SU(3)-flavor and heavy-flavor symmetries. Similarly, the spin-1/2 and spin-3/2 charmed baryons can also form a superfield S^μ within HQSS as

$$S^\mu \equiv -\frac{1}{\sqrt{3}}(\gamma^\mu + v^\mu)\gamma^5 B_6 + B_6^{*\mu}, \tag{11}$$

while the conjugate field $\bar{S}^\mu$ is defined as

$$\bar{S}^\mu \equiv S^{\mu\dagger}\gamma^0 = \frac{1}{\sqrt{3}}\bar{B}_6\gamma^5(\gamma^\mu + v^\mu) + \bar{B}_6^{*\mu}. \tag{12}$$

The $B_6(B_6^{*\mu})$ represents the matrix formed by the spin-1/2 (3/2) baryons which have the configuration of one heavy and two light quarks,

$$B_6 \equiv \begin{bmatrix} \Sigma^{++} & \frac{1}{\sqrt{2}}\Sigma^+ & \frac{1}{\sqrt{2}}\Xi'^+ \\ \frac{1}{\sqrt{2}}\Sigma^+ & \Sigma^0 & \frac{1}{\sqrt{2}}\Xi'^0 \\ \frac{1}{\sqrt{2}}\Xi'^+ & \frac{1}{\sqrt{2}}\Xi'^0 & \Omega^0 \end{bmatrix}. \tag{13}$$

In the above expressions, v^μ denotes the 4-velocity of the heavy meson or baryon, satisfying $v_\mu v^\mu = 1$. In the heavy quark limit ($m_Q \to \infty$), we adopt the static limit $v^\mu = (1, \vec{0})$. The symbol $\langle \ldots \rangle$ represents the trace over Dirac γ matrices, while $\mathrm{Tr}[\ldots]$ denotes the trace over flavor indices. The quantities V^μ and X^μ correspond to the vector and axial-vector currents, respectively, constructed from the light pseudoscalar mesons (see A 1 for details),

$$\begin{aligned} V^\mu &\equiv \frac{1}{2}(\xi^\dagger\partial^\mu\xi + \xi\partial^\mu\xi^\dagger), \\ X^\mu &\equiv \frac{1}{2}(\xi^\dagger\partial^\mu\xi - \xi\partial^\mu\xi^\dagger), \end{aligned} \tag{14}$$

where ξ is defined as

$$\xi \equiv \exp(\mathrm{i}\mathbb{P}/f_\pi) \tag{15}$$

with $\mathbb{P}$ the matrix of the pseudoscalar mesons,

$$\mathbb{P} \equiv \begin{bmatrix} \frac{\pi^0}{\sqrt{2}} + \frac{\eta^0}{\sqrt{6}} & \pi^+ & \mathrm{K}^+ \\ \pi^- & -\frac{\pi^0}{\sqrt{2}} + \frac{\eta^0}{\sqrt{6}} & \mathrm{K}^0 \\ \mathrm{K}^- & \bar{\mathrm{K}}^0 & -\frac{2}{\sqrt{6}}\eta^0 \end{bmatrix}, \tag{16}$$

TABLE II. The values of coupling constants used in the calculation.

g_S	β	g	λ
0.76	0.90	0.59	0.56 GeV^{-1}
l_S	β_S	g_1	λ_S
6.20	−1.74	0.94	−3.31 GeV^{-1}

and $f_\pi = 0.132$ GeV the pion decay constant [56,59]. In Eqs. (6)–(7), $F^{\mu\nu}$ is the tensor current constructed by the light vector mesons,

$$F^{\mu\nu} \equiv \partial^\mu \mathbb{V}'^\nu - \partial^\nu \mathbb{V}'^\mu + [\mathbb{V}'^\mu, \mathbb{V}'^\nu], \tag{17}$$

where

$$\mathbb{V}'^\mu \equiv \mathrm{i}g_V \mathbb{V}^\mu/\sqrt{2}, \tag{18}$$

with $g_V = m_\rho/f_\pi = 5.83$ [59,62,63] and the matrix for the light vector mesons,

$$\mathbb{V}^\mu \equiv \begin{bmatrix} \frac{\rho^0}{\sqrt{2}} + \frac{\omega^0}{\sqrt{2}} & \rho^+ & \mathrm{K}^{*+} \\ \rho^- & -\frac{\rho^0}{\sqrt{2}} + \frac{\omega^0}{\sqrt{2}} & \mathrm{K}^{*0} \\ \mathrm{K}^{*-} & \bar{\mathrm{K}}^{*0} & \phi^0 \end{bmatrix}^\mu. \tag{19}$$

In Table II, we provide the values for other coupling constants appearing in the Lagrangians [33,56,59–63].

To obtain the effective potentials in a nonrelativistic limit, we apply the Breit approximation

$$V = -\frac{\mathcal{M}}{\sqrt{\prod(2m_i)}\sqrt{\prod(2m_f)}}, \tag{20}$$

in which $m_i(m_f)$ is the mass of the incoming (outgoing) particle. The scattering amplitude $\mathcal{M}$ can be obtained by calculating the Feynman diagrams in Fig. 2 (refer to A 2 for the explicit Feynman rules). Through straightforward calculation, we obtain the effective potential $V(q)$ in momentum space (refer to A 3 for details). The corresponding coordinate-space potential is then derived via the Fourier transformation

$$V(r) = \hat{\mathcal{F}}[V(\mathbf{q})] = \int \frac{d^3\mathbf{q}}{(2\pi)^3} e^{\mathrm{i}\mathbf{q}\cdot\mathbf{r}} V(\mathbf{q}). \tag{21}$$

It is found that the effective potentials are classified into three types, i.e., the center force, spin-orbital force and tensor force. The latter two are well known to play crucial roles in nuclear physics. The spin-orbit force is essential for explaining the magic numbers in atomic nuclei, while the tensor force mixing the partial waves with l and $l \pm 2$ plays a key role in describing the weakly bound deuteron.

Overall, the effective potential can be written in the following general form:

$$V(r) = f_c(r)\mathcal{O}_{\rm cen} + f_{\rm SL}(r)\mathcal{O}_{\rm SL} + f_{\rm ten}(r)\mathcal{O}_{\rm ten}, \quad (22)$$

where $f_i(r)$ is a scalar function while $\mathcal{O}_i$ is the operator for each type of interactions.

However, the effective potential for exchanging a light pseudoscalar/vector meson is singular due to the following results:

$$\hat{\mathcal{F}}\left[\frac{\mathbf{q}^2}{\mathbf{q}^2+u^2}\right] = -4\pi\delta(\mathbf{r}) + f(r,u). \quad (23)$$

From a physical perspective, hadrons are not elementary particles but possess nontrivial internal structure. To account for this in theoretical calculations, a form factor is typically introduced as

$$F_n(\Lambda, m, q) = \left(\frac{\Lambda^2 - m^2}{\Lambda^2 - q^2}\right)^n, \quad (24)$$

which is called n-point form factor. In Eq. (24), q and m are the transferred 4-momentum and mass of the exchanged meson, respectively, and Λ is the momentum cutoff introduced to suppress the high-momentum contribution. In such a way, the singular behavior of the interaction potential can be regularized when two hadrons approach each other. In our calculation, we apply the monopole ($n = 1$) form factor,

$$V(r) = \int \frac{\mathrm{d}^3\mathbf{q}}{(2\pi)^3} e^{i\mathbf{q}\cdot\mathbf{r}} V(\mathbf{q}) F_1^2(\Lambda, m, q). \quad (25)$$

Note that $F_1(\Lambda, m, q) \to 1$ as $\Lambda \to \infty$, in which limit the form factor becomes trivial and the hadron is effectively treated as a pointlike particle. However, the appropriate value of Λ for a given calculation is not *a priori* known. In practice, one typically adopts values in the range $1.0 < \Lambda < 1.5$ GeV, which have been shown to accurately describe both the properties of the weakly bound deuteron and neutron-proton scattering within the framework of OBE model [64]. In the present work, we therefore adopt this range as the physically motivated choice for Λ.

The explicit expressions of spin currents and OBE potentials in coordinate space are given in Appendix B.

C. Isospin breaking

Essentially, isospin breaking originates from two fundamental sources: the strong interaction, arising from the mass difference between up and down quarks, and the electromagnetic interaction, arising from their charge difference. At the hadronic level, these effects manifest in several ways in the present study. First, the strong interaction contribution to isospin breaking is reflected in the mass differences among hadrons belonging to the same isospin multiplet—specifically, between $D^{(*)0}$ and $D^{(*)+}$, between π^0 and $\pi^\pm$, and among the $\Sigma_c^{(*)}$ states. Second, electromagnetic isospin breaking enters through the Coulomb interaction between charged $D^{(*)}$ and $\Sigma_c^{(*)}$ states. In principle, isospin breaking also affects the coupling constants for mesons with different I_3 projections within the same isospin multiplet. However, such effects are expected to be minor and are neglected in this work. Accordingly, we retain the SU(3)-flavor-symmetric Lagrangians introduced earlier. It is straightforward to incorporate the isospin breaking from the strong interaction. In the following, we will focus on the electromagnetic interaction, i.e., the Coulomb force between the charged $D^{(*)}$ and $\Sigma_c^{(*)}$.

Recall that the Coulomb interaction between two charged pointlike particles is

$$V_{\rm C}(r) = \frac{1}{\alpha}\frac{Z_1 Z_2}{r} \equiv Nk\frac{1}{r}, \quad (26)$$

where $k = 1/\alpha$ is the Coulomb constant and $N = Z_1 Z_2$, which cannot be applied directly to the hadrons with charge distributions. Due to the lack of experimental data, the charge distributions for most hadrons are not well determined. Nevertheless, the Coulomb interaction between charged hadrons can be modeled approximately using an exponential charge distribution. Alternatively, one may derive the Coulomb potential by employing an n-point form factor. The relationship between these two approaches is subtle. To clarify this, we derive the Coulomb force using both methods and compare the resulting potentials.

To compute the Coulomb interaction using the n-point form factor, we first rewrite the Coulomb force between two pointlike charge particles as

$$V_{\rm C}(r) = Nk\frac{e^{-\varepsilon r}}{r}, \qquad \varepsilon \to 0, \quad (27)$$

then perform an inverse Fourier transform of Eq. (27) to obtain the Coulomb potential in momentum space [65,66],

$$\tilde{V}_{\rm C}(\mathbf{q}) = \hat{\mathcal{F}}^{-1}[V_{\rm C}(r)] = Nk\frac{4\pi}{\mathbf{q}^2+\varepsilon^2} \xrightarrow{\varepsilon\to 0} Nk\frac{4\pi}{\mathbf{q}^2}. \quad (28)$$

Incorporating the n-point form factor $F_n(\eta, \mathbf{q})$ and performing the Fourier transform yields the modified Coulomb interaction:

$$\begin{aligned} V_{\rm C}^{2n}(r) &= \hat{\mathcal{F}}[F_n(\eta,\mathbf{q})\tilde{V}_{\rm C}(\mathbf{q})] \\ &= Nk\frac{1}{r}[1 - G_{2n}(\eta r)e^{-\eta r}], \end{aligned} \quad (29)$$

where [65]

$$F_n(\eta, \mathbf{q}) = \left(\frac{\eta^2}{\eta^2+\mathbf{q}^2}\right)^n \quad (30)$$

is the n-point form factor, and $G_n(x)$ is the nth form polynomial

$$\begin{aligned} G_0(x) &= 0, \\ G_1(x) &= 1, \\ G_2(x) &= 1+\frac{1}{2}x, \\ G_3(x) &= 1+\frac{5}{8}x+\frac{1}{8}x^2, \\ G_4(x) &= 1+\frac{11}{16}x+\frac{3}{16}x^2+\frac{1}{48}x^3, \\ &\cdots. \end{aligned} \tag{31}$$

On the other hand, given that a hadron state has sizable structure, an exponential charge distribution can be introduced for a charged hadron,

$$\rho_i(r) = Q_i\frac{a^3}{8\pi}e^{-ar}, \qquad (i=1,2), \tag{32}$$

in which Q_i is the charge of the ith hadron. The parameter is typically taken as $a = 2\sqrt{6}/r_{\mathrm{Q}}$ [51], where r_{Q} denotes the charge radius of the hadron.

Then, one can calculate the classical electromagnetic potential as

$$\begin{aligned} V_{\mathrm{C}}(r) &= k\int\frac{\rho_1(|\vec{r}_1|)\rho_2(|\vec{r}-\vec{r}_2|)}{|\vec{r}_1-\vec{r}_2|}\mathrm{d}\vec{r}_1\mathrm{d}\vec{r}_2 \\ &= Nk\frac{1}{r}[1-G_4(ar)e^{-ar}], \end{aligned} \tag{33}$$

where this G_4 function is defined the same as in Eq. (31).

It is clear that the integral result of Eq. (33) is exactly $V_{\mathrm{C}}^4(r)$ in Eq. (29), and the parameter a in Eq. (32) is just the cutoff η in Eq. (30). This result denotes that the two methods—either by applying an n-point form factor, or by applying an exponential charge distribution on the original Coulomb interaction—are equivalent. Besides, $V_{\mathrm{C}}^2(r)$ is the potential calculated by applying an exponential charge distribution for one hadron and a pointlike charged hadron, while $V_{\mathrm{C}}^0(r)$ represents just the original Coulomb interaction between two pointlike charged particles as Eq. (26).

The charge radius r_{Q} of most heavy hadrons has not been determined experimentally and can only be estimated via phenomenological approaches. As a rough reference, a charge radius of 0.3–0.4 fm was obtained for the doubly charmed baryon Ξ_{cc}^{++} in Ref. [67]. Although the internal structure of the molecular $D^{(*)}\Sigma_c^{(*)}$ system studied here differs from that of the compact Ξ_{cc} baryon, this value still gives a reasonable estimate for the order of magnitude of the charge radius. In this work, we adopt the empirical choice $a \sim 2\Lambda$, where Λ denotes the momentum cutoff in the OBE interaction. This choice is consistent with the relation $r_Q = \Lambda/\sqrt{6}$ given in Ref. [68].

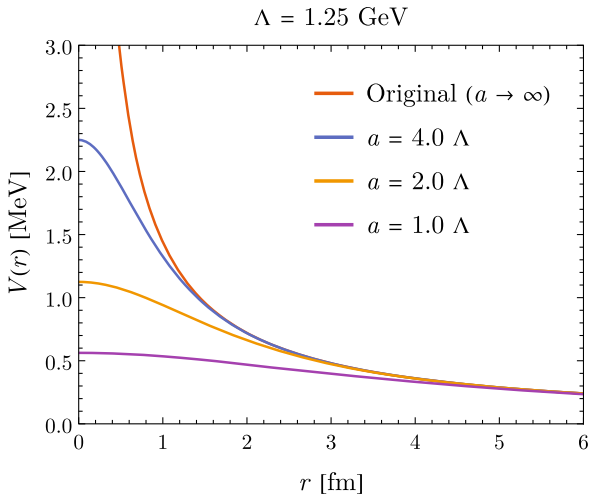


FIG. 3. Coulomb interaction between two charged pointlike particles and the ones between charged hadrons calculated using Eq. (33). For the latter, three cutoff values are adopted as $a = 1.0\Lambda, 2.0\Lambda, 4.0\Lambda$, with $\Lambda = 1.25$ GeV.

In Fig. 3, we present the Coulomb potential calculated from Eq. (33), together with the pointlike Coulomb potential for comparison. To examine the dependence on the cutoff parameter a, we consider three values, $a = 1.0\Lambda$, 2.0Λ, and 4.0Λ, with a typical $\Lambda = 1.25$ GeV. The results show that the Coulomb potential exhibits only a weak dependence on a for $r > 1.0$ fm. However, the cutoff plays an essential role in regularizing the $r \to 0$ divergence inherent to the pointlike interaction.

D. Schrödinger equation with isospin breaking

Since the interaction between two particles depends solely on their relative distance, a two-body system has spherical symmetry, i.e., one can separate the radial part of the wave function from its angular part. After integrating out the angular degrees of freedom, the radial Schrödinger equation takes the form

$$\left[-\frac{1}{2\mu}\partial_r{}^2+\frac{l(l+1)}{2\mu r^2}+V(r)\right]u(r) = Eu(r), \tag{34}$$

with $\mu = m_1m_2/(m_1+m_2)$, the reduced mass, and $u(r) = rR(r)$, the modified radial wave function. l and $V(r)$ represent the quantum numbers of orbital angular momentum and the interaction potential, respectively. For this case we include the isospin breaking, i.e., the Coulomb interaction between charged hadrons, the threshold difference of $D^{(*)}\Sigma_c^{(*)}$ belonging to the same isospin multiplet, and the matrix element of Hamiltonian is expressed as

$$H_{pq} = \langle\mathcal{P}|\hat{H}|\mathcal{Q}\rangle = T_{pq}+V_{pq}+\Delta M_{pq}, \tag{35}$$

where $\mathcal{P}$ and $\mathcal{Q}$ are two partial wave channels. The kinetic energy is always diagonal and can be written as

$$T_{pq} = -\frac{1}{2\mu_p}\partial_r^2\delta_{pq} + \frac{l_p(l_p+1)}{2\mu_p r^2}\delta_{pq}, \tag{36}$$

where μ_p and l_p are the reduced mass and quantum number of orbital angular momentum in the $\mathcal{P}$ channel, respectively. The second term is the centrifugal potential, which is positive and grows with increasing l_p.

The effective potential includes the strong interaction from exchanging a light meson and the Coulomb interaction,

$$V_{pq}(r) = V_{pq}^{\mathrm{OBE}}(r) + V_{pq}^{\mathrm{C}}(r). \tag{37}$$

To illustrate the construction of the strong interaction potential matrix, we consider the $D^*\Sigma_c$ system in the isospin state $|I, I_3\rangle = |1/2, 1/2\rangle$. In the basis $D^{*+}\Sigma_c^+, D^{*0}\Sigma_c^{++}$, the strong interaction potential matrix is expressed as

$$V^{\mathrm{OBE}}(r) = \begin{bmatrix} V_{11}^{\mathrm{OBE}}(r) & V_{12}^{\mathrm{OBE}}(r) \\ V_{21}^{\mathrm{OBE}}(r) & V_{22}^{\mathrm{OBE}}(r) \end{bmatrix}, \tag{38}$$

where

$$\begin{aligned} V_{11}^{\mathrm{OBE}}(r) &= \langle D^{*+}\Sigma_c^+|\hat{V}^{\mathrm{OBE}}(r)|D^{*+}\Sigma_c^+\rangle, \\ V_{12}^{\mathrm{OBE}}(r) &= \langle D^{*+}\Sigma_c^+|\hat{V}^{\mathrm{OBE}}(r)|D^{*0}\Sigma_c^{++}\rangle, \\ V_{22}^{\mathrm{OBE}}(r) &= \langle D^{*0}\Sigma_c^{++}|\hat{V}^{\mathrm{OBE}}(r)|D^{*0}\Sigma_c^{++}\rangle. \end{aligned}$$

The matrix of Coulomb interaction is expressed as

$$V^{\mathrm{C}}(r) = \begin{bmatrix} V_{11}^{\mathrm{C}}(r) & 0 \\ 0 & 0 \end{bmatrix}, \tag{39}$$

with $V_{11}^{\mathrm{C}}(r) = \langle D^{*+}\Sigma_c^+|\hat{V}^{\mathrm{C}}(r)|D^{*+}\Sigma_c^+\rangle$. Since D^{*0} is neutral, all remaining matrix elements of $V^{\mathrm{C}}(r)$ vanish.

The threshold difference is given by

$$\Delta M_{pq} = \delta M_p \delta_{pq}, \qquad \delta M_p = M_p - M_{\mathrm{min}}, \tag{40}$$

where M_p is the mass threshold of the pth channel, and M_{min} is the lowest threshold among all considered flavor channels.

When mixing between different partial waves is taken into account, each isospin state generally encompasses multiple partial-wave components. For instance, the $D^*\Sigma_c$ system with $|I, I_3\rangle = |1/2, 1/2\rangle$ and $J^P = 1/2^-$ involves two partial waves: $^2S_{1/2}$ and $^4D_{1/2}$. In such cases, each element of the potential matrix becomes a 2×2 submatrix in the partial-wave bases.

Alternatively, one can also write the potential matrix in the isospin bases, which is easily obtained from Eq. (38) via the following orthogonal transformation:

$$V^{\mathrm{iso}}(r) = UV(r)U^{-1}, \tag{41}$$

where U is the transform matrix. For the state with $I_3 = 1/2$,

$$U = \begin{pmatrix} \sqrt{\frac{1}{3}} & -\sqrt{\frac{2}{3}} \\ \sqrt{\frac{2}{3}} & \sqrt{\frac{1}{3}} \end{pmatrix}, \qquad U^{-1} = U^{\mathrm{T}}. \tag{42}$$

Firstly, we write the specific expression of potential matrix Eq. (38) as

$$V(r) = V_\sigma(r)\hat{\mathbf{I}} + V_8(r), \tag{43}$$

$$V_8(r) = \begin{bmatrix} \frac{V_\eta(r)+3V_\omega(r)}{6} & -\frac{V_\pi(r)+V_\rho(r)}{\sqrt{2}} \\ -\frac{V_\pi(r)+V_\rho(r)}{\sqrt{2}} & \frac{V_\eta(r)+3V_\omega(r)+3V_\pi(r)+V_\rho(r)}{6} \end{bmatrix}, \tag{44}$$

where $V_{\sigma,\pi,\rho,\eta,\omega}$ is the potential for exchanging a σ, π, ρ, η, or ω meson. Performing the transformation as in Eq. (41), the potential matrix converts into

$$V^{\mathrm{iso}}(r) = V_\sigma(r)\hat{\mathbf{I}} + V_8^{\mathrm{iso}}(r), \tag{45}$$

$$\begin{aligned} V_8^{\mathrm{iso}}(r) = \mathbf{Diag}\Bigg[&\left(\frac{1}{6}V_\eta(r) + \frac{1}{2}V_\omega(r)\right) + (V_\pi(r) + V_\rho(r)), \\ &\left(\frac{1}{6}V_\eta(r) + \frac{1}{2}V_\omega(r)\right) - \frac{1}{2}(V_\pi(r) + V_\rho(r))\Bigg], \end{aligned} \tag{46}$$

or in a more compact form

$$V^{\mathrm{iso}}(r) = \begin{bmatrix} V_{11}^{D^*\Sigma_c}(r) & 0 \\ 0 & V_{22}^{D^*\Sigma_c}(r) \end{bmatrix}, \tag{47}$$

in which

$$\begin{aligned} V_{11}^{D^*\Sigma_c}(r) &= \langle 1/2, 1/2|\hat{V}^{D^*\Sigma_c}(r)|1/2, 1/2\rangle, \\ V_{22}^{D^*\Sigma_c}(r) &= \langle 3/2, 1/2|\hat{V}^{D^*\Sigma_c}(r)|3/2, 1/2\rangle. \end{aligned} \tag{48}$$

It is clear that the isospin-1/2 and -3/2 states will decouple in the isospin symmetry limit. Applying the same transformation to the two isospin-breaking terms yields

$$V_{\mathrm{C}}^{\mathrm{iso}}(r) = UV_{\mathrm{C}}(r)U^{-1} = \begin{pmatrix} \frac{1}{3} & \frac{\sqrt{2}}{3} \\ \frac{\sqrt{2}}{3} & \frac{2}{3} \end{pmatrix} V_{\mathrm{C}}(r), \tag{49}$$

and

$$\Delta M^{\rm iso} = U\Delta M U^{-1} = \begin{pmatrix} \frac{1}{3} & \frac{\sqrt{2}}{3} \\ \frac{\sqrt{2}}{3} & \frac{2}{3} \end{pmatrix} \Delta M. \quad (50)$$

It is now evident from Eqs. (49)–(50) that the presence of isospin-breaking terms induces mixing between the $I = 1/2$ and $I = 3/2$ states. Consequently, total isospin I is no longer a good quantum number, although its third component I_3 remains conserved.

III. NUMERICAL RESULTS

In this section, we present our numerical results and quantitative analyses. We first show the results obtained under isospin symmetry, followed by those with isospin breaking explicitly included. The effects of isospin breaking can then be assessed by comparing the two sets of results.

Before including isospin-breaking effects, we first compare our baseline results with earlier studies on the $D^{(*)}\Sigma_c^{(*)}$ systems. In Ref. [34], the authors studied the spectrum for isospin $I = 1/2$ and concluded that bound states can emerge in numerous channels. In Ref. [33] the authors carried out a thorough coupled-channel analysis for both $I = 1/2$ and $I = 3/2$ states. Their results demonstrated that within the typical cutoff range $\Lambda \sim 1.0$–1.5 GeV, the $I = 1/2$ configurations tend to form bound states readily, whereas certain $I = 3/2$ states can also develop weak binding for a larger cutoff value. Our results obtained without isospin breaking are in overall agreement with these previous findings. The consistency validates our theoretical framework as a reliable baseline prior to introducing Coulomb-induced corrections.

A. The $D\Sigma_c$ systems

The S-wave ground state of the $D\Sigma_c$ system carries spin-parity $J^P = 1/2^-$, involving only the partial wave $^2S_{1/2}$. Its total isospin can be either $I = 1/2$ or $3/2$. At tree level, the absence of $D\mathcal{P}D$ interaction vertex forbids coupling to diagrams involving a light pseudoscalar meson $\mathcal{P}$ (e.g., a pion) exchanged between the D and Σ_c. Consequently, within the OBE potential model, the interaction proceeds solely via the exchange of heavier scalar and vector mesons, such as σ, ρ, and ω, which generate the medium- and short-range forces.

As shown in Table III, our numerical results indicate that the isospin-$1/2$ $D\Sigma_c$ system can form a loosely bound state. Under the isospin symmetry, the binding energy ranges from 0.36 to 13.69 MeV, and the corresponding root-mean-square (rms) radius ranges from 4.75 to 1.12 fm, for the momentum cutoff varied in the range $\Lambda = 1.14$–1.30 GeV. These binding properties suggest that this state can be regarded as a typical hadronic molecule. In contrast, no bound state is found for the isospin-$3/2$ $D\Sigma_c$ system for cutoff values up to 5.0 GeV.

TABLE III. Binding solutions of the $D\Sigma_c$ system. The two cases I and II mean without (w/o) and with (w/) isospin breaking. Λ, E_b, and $r_{\rm rms}$ are the momentum cutoff (in units of GeV), binding energy (in units of MeV) and root-mean-square (rms) radius (in units of fm), respectively. $\times$ means no bound state when $\Lambda < 5.0$ GeV. The obtained bound states are in pure S-wave.

$\vert I, I_3\rangle$	Cases	Λ (GeV)	E_b (MeV)	$r_{\rm rms}$ (fm)
$\vert 1/2, 1/2\rangle$	I (w/o)	1.14	0.36	4.75
		1.25	7.67	1.41
		1.30	13.69	1.12
	II (w/)	1.18	0.41	2.67
		1.25	5.90	1.44
		1.30	11.83	1.14
$\vert 3/2, 1/2\rangle$			$\times$	
$\vert 3/2, 3/2\rangle$			$\times$	

When isospin breaking is included, both the binding energy and the rms radius of the isospin-$1/2$ $D\Sigma_c$ state shift appreciably, indicating sizable isospin-breaking effects in this hadronic molecular candidate. For instance, at a cutoff value of $\Lambda = 1.25$ GeV, the rms radius increases from 1.41 fm to 1.44 fm, while the binding energy decreases from 7.67 MeV to 5.90 MeV upon the inclusion of isospin breaking. This corresponds to a roughly 23% correction to the binding energy.

B. The $D\Sigma_c^*$ systems

The ground state of the $D\Sigma_c^*$ system with $J^P = 3/2^-$ involves two partial waves: $^4S_{3/2}$ and $^4D_{3/2}$. However, we find that the D-wave contribution is negligible in our calculation.

The numerical results of $D\Sigma_c^*$ are shown in Table IV. Similarly to the results of the $D\Sigma_c$ system, the isospin-$1/2$ $D\Sigma_c^*$ can form a loosely bound state. Under the isospin

TABLE IV. Binding solutions of the $D\Sigma_c^*$ system. Λ, E_b and $r_{\rm rms}$ are the momentum cutoff (in units of GeV), binding energy (in units of MeV) and rms radius (in units of fm), respectively. It should be mentioned that the obtained bound state is pure S-wave. $\times$ mean no bound states for $\Lambda < 5.0$ GeV.

$\vert I, I_3\rangle$	Cases	Λ (GeV)	E_b (MeV)	r_{rms} (fm)
$\vert 1/2, 1/2\rangle$	I (w/o)	1.14	0.45	4.44
		1.25	8.08	1.38
		1.30	14.27	1.10
	II (w/)	1.18	0.50	2.53
		1.25	6.20	1.41
		1.30	12.29	1.12
$\vert 3/2, 1/2\rangle$			$\times$	
$\vert 3/2, 3/2\rangle$			$\times$	

symmetry, the binding energy and rms radius of this state are 0.45 to 14.27 MeV and 4.44 to 1.10 fm, respectively, when the momentum cutoff varied in the range $\Lambda =$ 1.14–1.30 GeV. However, we could not obtain any binding solutions for the isospin-3/2 $D\Sigma_c^*$ system when the momentum cutoff is smaller than 5.0 GeV.

Taking into account the isospin breaking, the binding energy and rms radius of the isospin-1/2 $D\Sigma_c^*$ state also exhibit noticeable shifts. Specifically, at $\Lambda = 1.25$ GeV, the rms radius increases from 1.38 fm to 1.41 fm, while the binding energy decreases from 8.08 MeV to 6.20 MeV, indicating about 23% isospin-breaking correction to the binding energy.

C. The $D^*\Sigma_c$ systems

The spin-parity of the $D^*\Sigma_c$ system could be $J^P = 1/2^-$ or $3/2^-$ in the ground states. As illustrated in Table I, we shall consider the $^2S_{1/2}$ and $^4D_{1/2}$ partial waves for the $J^P = 1/2^-$ channel, and the $^4S_{3/2}$, $^2D_{3/2}$ and $^4D_{3/2}$ partial waves for the $J^P = 3/2^-$ channel. We present the numerical results for the $D^*\Sigma_c$ systems with $J^P = 1/2^-$ and $3/2^-$ in Tables V and VI, respectively.

The isospin-3/2 $D^*\Sigma_c$ with $J^P = 1/2^-$ can also form a loosely bound state with binding energy 0.22–18.77 MeV and rms radius $5.11 - 0.87$ fm for the momentum cutoff tuned to 1.40–1.90 GeV, in the isospin symmetry limit. It is predominantly $^2S_{1/2}$, with a probability larger than 99%, and minor contribution from $^4D_{1/2}$, less than 1%. The state $D^{*+}\Sigma_c^{++}$ ($|I, I_3\rangle = |3/2, 3/2\rangle$) is particularly interesting since it has three positive unit charges and cannot be formed by three quarks in the traditional way of the quark model. From this perspective, it can be taken as an "absolute" exotic hadronic state once established.

Our results show that the $D^*\Sigma_c$ system with spin-parity $J^P = 1/2^-$ and isospin $I = 1/2$ can form a loosely bound state. In the isospin symmetry case, with the momentum cutoff varied in the range $\Lambda = 1.15$–1.25 GeV, the binding energy ranges from 0.53 to 14.38 MeV and the corresponding rms radius from 4.33 to 1.14 fm, characteristic of a typical hadronic molecule. This state is predominantly a $^2S_{1/2}$ component, with a probability of 86.72%—96.34%, and a minor admixture of the $^4D_{1/2}$ component (3.66%—13.28%).

The isospin-3/2 $D^*\Sigma_c$ system with $J^P = 1/2^-$ can also bind in the isospin symmetry. For the cutoff value $\Lambda = 1.40$–1.90 GeV, the binding energy ranges from 0.22 to 18.77 MeV and the rms radius from 5.11 to 0.87 fm. This loosely bound state is dominated by the $^2S_{1/2}$ with a probability exceeding 99%, while the $^4D_{1/2}$ contribution is below 1%. The triply charged state $D^{*+}\Sigma_c^{++}$ with $|I, I_3\rangle = |3/2, 3/2\rangle$ is especially interesting, since this state cannot be formed from three quarks in the conventional quark model. It would thus represent a genuinely exotic baryon if observed experimentally.

The inclusion of isospin breaking leads to significant modifications in the binding energy. For the isospin-1/2 case with $\Lambda = 1.22$ GeV, the analyses show that the isospin-breaking effect provides around 17% correction to the binding energy, a sizable effect given the shallow nature of the molecular state.

TABLE V. Binding solutions of the $D^*\Sigma_c$ system with $J^P = 1/2^-$. The cases I and II mean without (w/o) and with (w/) isospin breaking, respectively. Λ, E_b, and $r_{\rm rms}$ are respective the momentum cutoff (in units of GeV), binding energy (in units of MeV) and rms radius (in units of fm). $P_i(\%)$ is the probability of the channel i, with $i = |^2S_{1/2}\rangle$ or $|^4D_{1/2}\rangle$.

$\lvert I, I_3\rangle$	Cases	Λ (GeV)	E_b (MeV)	$r_{\rm rms}$ (fm)	$P_i(\%)$	
$\lvert 1/2, 1/2\rangle$	I (w/o)	1.16	0.53	4.33	96.34	3.66
		1.22	7.16	1.49	89.18	10.82
		1.25	14.38	1.14	86.72	13.28
	II (w/)	1.17	0.03	3.70	95.42	4.58
		1.22	5.92	1.53	89.29	10.71
		1.25	13.02	1.15	86.76	13.24
$\lvert 3/2, 1/2\rangle$	I (w/o)	1.40	0.22	5.11	99.78	0.22
		1.72	8.44	1.22	99.40	0.60
		1.90	18.77	0.87	99.30	0.70
	II (w/)	1.55	0.15	2.42	99.58	0.42
		1.72	5.51	1.30	99.41	0.59
		1.90	15.41	0.90	99.30	0.70
$\lvert 3/2, 3/2\rangle$	I (w/o)	Same as those of $\lvert I, I_3\rangle = \lvert 3/2, 1/2\rangle$ in case I				
	II (w/)	1.60	0.59	2.94	99.59	0.41
		1.72	3.99	1.52	99.43	0.57
		1.90	12.96	0.96	99.30	0.70

TABLE VI. Binding solutions of the $D^*\Sigma_c$ system with $J^P = 3/2^-$. I and II denote the cases without (w/o) and with (w/) isospin breaking, respectively. Λ, E_b and $r_{\rm rms}$ are the momentum cutoff (in units of GeV), the binding energy (in units of MeV) and rms radius (in units of fm). $P_i(\%)$ is the probability of the channel i, with $i = |^4S_{3/2}\rangle, |^2D_{3/2}\rangle$ or $|^4D_{3/2}\rangle$.

$\|I, I_3\rangle$	Cases	Λ (GeV)	E_b (MeV)	$r_{\rm rms}$ (fm)	$P_i(\%)$		
$\|1/2, 1/2\rangle$	I (w/o)	0.91	0.33	4.82	97.86	0.49	1.65
		1.00	7.58	1.46	94.37	1.28	4.35
		1.04	13.88	1.18	93.33	1.50	5.16
	II (w/)	0.93	0.10	3.47	96.98	0.70	2.33
		1.00	6.35	1.49	94.39	1.27	4.34
		1.04	12.57	1.19	93.33	1.51	5.16
$\|3/2, 1/2\rangle$	I (w/o)	3.90	0.82	3.52	98.08	0.30	1.62
		4.70	9.73	1.20	94.86	0.74	4.40
		4.90	14.25	1.02	94.11	0.84	5.05
	II (w/)	4.20	0.33	2.41	97.14	0.43	2.43
		4.70	5.12	1.44	95.40	0.67	3.93
		4.90	11.06	1.06	94.24	0.82	4.94
$\|3/2, 3/2\rangle$	I (w/o)	Same as those of $\|I, I_3\rangle = \|3/2, 1/2\rangle$ in case I					
	II (w/)	4.30	0.54	3.13	97.47	0.38	2.15
		4.70	5.12	1.44	95.40	0.67	3.93
		4.90	8.98	1.16	94.54	0.78	4.68

For the isospin-3/2 case, the states $|I, I_3\rangle = |3/2, 1/2\rangle$ and $|3/2, 3/2\rangle$ are degenerate under isospin symmetry. This degeneration is dissolved once isospin breaking is introduced, and the resulting splitting provides a measure of the strength of isospin-breaking effects. As in the isospin-1/2 case, the binding of the $D^*\Sigma_c$ state with $J^P = 1/2^-$ and $|I, I_3\rangle = |3/2, 1/2\rangle$ becomes weaker upon the inclusion of isospin breaking, corresponding to exceeding 30% binding energy correction for this loosely bound molecular state (see Table V).

In the $J^P = 3/2^-$ sector, the isospin-1/2 $D^*\Sigma_c$ system forms a weakly bound state in the isospin symmetry, with binding energy 0.33–13.88 MeV and rms radius 4.82–1.18 fm for $\Lambda = 0.91$–1.04 GeV. This state is predominantly $^4S_{3/2}$, with small admixtures from $^2D_{3/2}$ and $^4D_{3/2}$. No bound state is found for the isospin-3/2 configuration within the physically relevant cutoff region. When isospin breaking is included, the binding of the isospin-1/2 state weakens, as shown in Table VI.

D. The $D^*\Sigma_c^*$ systems

The $D^*\Sigma_c^*$ system can form ground states with spin-parity $J^P = 1/2^-$, $3/2^-$, and $5/2^-$. In addition to the dominant S-wave configurations, we also include higher partial waves that can couple via the tensor force. Specifically, we consider the partial waves $^2S_{1/2}$, $^4D_{1/2}$, $^6D_{1/2}$ for $J^P = 1/2^-$, $^4S_{3/2}, ^2D_{3/2}, ^4D_{3/2}, ^6D_{3/2}$ for $J^P = 3/2^-$, and $^6S_{5/2}, ^2D_{5/2}, ^4D_{5/2}, ^6D_{5/2}$ for $J^P = 5/2^-$, see Table I. We present the numerical results in Tables VII–IX for $J^P = 1/2^-$, $3/2^-$ and $5/2^-$, respectively.

The numerical results demonstrate that the $D^*\Sigma_c^*$ with $J^P = 1/2^-$ and $I = 1/2$ can form a hadronic molecular state. Its binding energy and rms radius are respective 0.26–14.34 MeV and $5.32 - 1.20$ fm for the momentum cutoff $\Lambda = 1.09$–1.19 GeV in the isospin symmetry limit. It dominantly lies in state $|^2S_{1/2}\rangle$ (95.90%–80.54%), and small contributions stem from $^4D_{1/2}$ (1.95%–8.23%) and $^4D_{1/2}$ (2.16%–11.22%). The situation for the isospin-3/2 case is similar. Under isospin symmetry, the binding energy and rms radius for the $|I, I_3\rangle = |3/2, 1/2\rangle$ state are 0.36–14.81 MeV and $4.53 - 1.98$ fm, respectively, when the momentum cutoff is set to $\Lambda = 1.20$–1.55 GeV. The contribution of the dominant channel $^2S_{1/2}$ is around 90%. With isospin symmetry, the states $|I, I_3\rangle = |3/2, 1/2\rangle$ and $|3/2, 3/2\rangle$ are degenerate.

Once the isospin breaking is included, the rms radius of $D^*\Sigma_c^*$ with isospin-1/2 increases from 1.56 fm to 1.59 fm when $\Lambda = 1.16$ GeV. Accordingly, the binding energy decreases from 7.12 MeV to 5.82 MeV, which indicates that the isospin breaking leads to a relative correction of 18.26% to the binding energy. The effect is even more pronounced for the isospin-3/2 states. For example, in the $|I, I_3\rangle = |3/2, 1/2\rangle$ channel with $\Lambda = 1.45$ GeV, the binding energy drops from 8.45 MeV to 5.41 MeV upon the inclusion of isospin breaking, yielding a relative change of approximately 36% to the binding energy.

TABLE VII. Binding solutions of the $D^*\Sigma_c^*$ system with $J^P = 1/2^-$. I and II denote the cases without (w/o) and with (w/) isospin breaking, respectively. Λ, E_b and $r_{\rm rms}$ are the respective momentum cutoff (in units of GeV), binding energy (in units of MeV) and rms radius (in units of fm). $P_i(\%)$ is the probability of the channel i, with $i = |^2S_{1/2}\rangle$, $|^4D_{1/2}\rangle$ or $|^6D_{1/2}\rangle$.

$\|I, I_3\rangle$	Cases	Λ (GeV)	E_b (MeV)	$r_{\rm rms}$ (fm)	$P_i(\%)$		
$\|1/2, 1/2\rangle$	I (w/o)	1.09	0.26	5.32	95.90	1.95	2.14
		1.16	7.12	1.56	84.10	6.92	8.98
		1.19	14.34	1.20	80.54	8.23	11.22
	II (w/)	1.12	0.67	2.88	90.93	4.16	4.91
		1.16	5.82	1.59	84.24	6.87	8.89
		1.19	12.94	1.21	80.60	8.21	11.19
$\|3/2, 1/2\rangle$	I (w/o)	1.20	0.36	4.53	99.56	0.26	0.17
		1.45	8.45	1.24	99.01	0.61	0.38
		1.55	14.81	0.98	98.92	0.67	0.42
	II (w/)	1.32	0.28	2.24	99.24	0.46	0.30
		1.45	5.41	1.30	99.02	0.60	0.38
		1.55	11.51	1.01	98.92	0.67	0.42
$\|3/2, 3/2\rangle$	I (w/o)	Same as those of $\|I, I_3\rangle = \|3/2, 1/2\rangle$ in case I					
	II (w/)	1.34	0.48	3.10	99.33	0.41	0.27
		1.45	4.25	1.49	99.04	0.59	0.37
		1.55	9.79	1.09	98.92	0.67	0.42

TABLE VIII. Binding solutions of the $D^*\Sigma_c^*$ system with $J^P = 3/2^-$. I and II denote the cases without (w/o) and with (w/) isospin breaking, respectively. Λ, E_b, and $r_{\rm rms}$ are the momentum cutoff (in units of GeV), binding energy (in units of MeV) and rms radius (in units of fm). $P_i(\%)$ is the probability of the channel i, with $i = |^4S_{3/2}\rangle, |^2D_{3/2}\rangle, |^4D_{3/2}\rangle$ or $|^6D_{3/2}\rangle$.

$\|I, I_3\rangle$	Cases	Λ (GeV)	E_b (MeV)	$r_{\rm rms}$ (fm)	$P_i(\%)$			
$\|1/2, 1/2\rangle$	I (w/o)	1.14	7.62	1.50	91.46	2.93	4.87	0.74
		1.18	15.84	1.14	89.71	3.53	5.84	0.91
	II (w/)	1.08	0.09	3.44	95.67	1.48	2.49	0.35
		1.14	6.29	1.52	91.52	2.91	4.84	0.73
		1.18	14.41	1.15	89.73	3.53	5.83	0.91
$\|3/2, 1/2\rangle$	I (w/o)	1.80	0.19	5.33	99.38	0.17	0.41	0.05
		2.30	9.02	1.20	97.70	0.61	1.52	0.17
		2.50	16.96	0.92	97.24	0.73	1.83	0.20
	II (w/)	2.05	0.17	2.31	98.53	0.39	0.97	0.11
		2.30	5.81	1.27	97.75	0.59	1.48	0.17
		2.50	13.40	0.95	97.26	0.72	1.81	0.20
$\|3/2, 3/2\rangle$	I (w/o)	Same as those of $\|I, I_3\rangle = \|3/2, 3/2\rangle$ in case I						
	II (w/)	2.10	0.47	3.15	98.71	0.34	0.85	0.10
		2.30	4.38	1.48	97.89	0.56	1.40	0.16
		2.50	11.18	1.03	97.33	0.70	1.77	0.20

This enhanced sensitivity can be understood from the effective charge product $N_{\rm eff}$ associated with each state. For the isospin-1/2 configuration, the repulsive Coulomb interaction corresponds to $N_{\rm eff} = 1/3$, whereas for the $|I, I_3\rangle = |3/2, 3/2\rangle$ state $D^{*+}\Sigma_c^{*++}$, one has $N_{\rm eff} = 2$. The stronger Coulomb repulsion in the latter case leads to a more significant impact on the binding energy. Among all sources of isospin breaking considered, we find that the electromagnetic interaction plays the dominant role.

TABLE IX. Binding solutions of the $D^*\Sigma_c^*$ system with $J^P = 5/2^-$. I and II denote cases without (w/o) and with (w/) isospin breaking, respectively. Λ, E_b and $r_{\rm rms}$ are the respective momentum cutoff (in units of GeV), binding energy (in units of MeV) and rms radius (in units of fm). P_i is the probability of the channel i, with $i = |^6S_{5/2}\rangle, |^2D_{5/2}\rangle, |^4D_{5/2}\rangle$ or $|^6D_{5/2}\rangle$.

$\lvert I, I_3\rangle$	Cases	Λ (GeV)	E_b (MeV)	$r_{\rm rms}(fm)$	$P_i(\%)$			
$\lvert 1/2, 1/2\rangle$	I (w/o)	0.85	0.28	4.94	98.22	0.25	0.07	1.45
		0.95	8.00	1.41	95.45	0.65	0.18	3.72
		1.00	15.79	1.11	94.54	0.78	0.21	4.47
	II (w/)	0.88	0.32	2.99	97.18	0.40	0.11	2.31
		0.95	6.65	1.43	95.46	0.65	0.18	3.72
		1.00	14.35	1.12	94.53	0.78	0.21	4.47
$\lvert 3/2, 1/2\rangle$	I (w/o)	3.60	0.51	4.23	97.93	0.11	0.06	1.90
		4.30	8.22	1.30	93.41	0.26	0.20	6.12
		4.60	16.00	0.98	91.58	0.30	0.26	7.85
	II (w/)	4.00	0.78	2.12	95.67	0.19	0.14	4.01
		4.30	5.18	1.37	93.64	0.26	0.20	5.91
		4.60	12.63	1.02	91.74	0.30	0.26	7.71
$\lvert 3/2, 3/2\rangle$	I (w/o)	Same as those of $\lvert I, I_3\rangle = \lvert 3/2, 1/2\rangle$ in case I						
	II (w/)	4.05	0.88	2.73	96.23	0.17	0.12	3.48
		4.30	4.05	1.59	94.19	0.24	0.18	5.40
		4.60	10.78	1.09	92.09	0.29	0.25	7.37

For the $J^P = 3/2^-$ channel with isospin $I = 1/2$, a weakly bound state is also found for cutoff values around 1.10 GeV. Specifically, with isospin symmetry, the rms radius and binding energy are 1.50 fm and 7.62 MeV, respectively, for $\Lambda = 1.14$ GeV, and the results have a mild dependence on the momentum cutoff. This state thus represents a good hadronic molecular candidate. In contrast, for the isospin-3/2 configuration with the same $J^P = 3/2^-$, no bound solution is obtained unless the cutoff exceeds 1.80 GeV. As in the $J^P = 1/2^-$ case, isospin breaking weakens the binding of $D^*\Sigma_c^*$ with $J^P = 3/2^-$ and isospin-1/2. At $\Lambda = 1.14$ GeV, the binding energy decreases from 7.62 MeV to 6.29 MeV upon the inclusion of isospin breaking, corresponding to a relative correction of 17.45%.

For the state with $J^P = 5/2^-$ and isospin-1/2, a loosely bound state is obtained when $\Lambda \sim 1.0$ GeV. Within isospin symmetry, its rms radius and binding energy are 4.94 – 1.11 fm and 0.28–15.79 MeV, respectively, when $\Lambda = 0.85$–1.00 GeV. It mainly lies in the partial wave $^6S_{5/2}$, with a probability of 98.22%–94.54%. Minor contributions arise from the $^2D_{5/2}$ and $^4D_{5/2}$ (less than 1%), and a small contribution stems from the partial wave $^6D_{5/2}$ (1.45%–4.47%). In contrast, no bound solution is found for the isospin-3/2 configuration unless Λ is increased to as large as 4.0 GeV. When isospin breaking is included, the binding of the isospin-1/2 $D^*\Sigma_c^*$ state weakens. For instance, at a fixed cutoff $\Lambda = 0.95$ GeV, the binding energy decreases from 8.00 MeV to 6.65 MeV upon the inclusion of isospin breaking, corresponding to a relative correction of 16.88%. In contrast, the probabilities of the individual partial waves remain largely unaffected by isospin breaking.

E. The isospin-breaking angle

Under isospin symmetry, all states within a given isospin multiplet $|I, I_3\rangle$ are degenerate. Once isospin breaking is introduced, this degeneracy is dissolved, and states with different total isospin I but the same third component I_3 can mix. Consequently, total isospin I is no longer a good quantum number, although I_3 remains conserved. In this subsection, we introduce a mixing angle that quantifies the degree of isospin mixing induced by isospin breaking. This angle also serves as a measure of the strength of isospin-breaking effects.

To compute the mixing angle, we consider the two isospin states $|I, I_3\rangle = |1/2, 1/2\rangle$ and $|3/2, 1/2\rangle$ of the $D^{(*)}\Sigma_c^{(*)}$ system. With these two bases, the off diagonal matrix elements of the Hamiltonian are nonzero, leading to the mixing of these two isospin states. The mixing angle θ is defined as

$$|D^{(*)}\Sigma_c^{(*)}\rangle \equiv \cos\theta |D^{(*)}\Sigma_c^{(*)}\rangle^{(I,I_3)=(1/2,1/2)} + \sin\theta |D^{(*)}\Sigma_c^{(*)}\rangle^{(I,I_3)=(3/2,1/2)}, \quad (51)$$

from which

TABLE X. The isospin-breaking angle θ of the $D^{(*)}\Sigma_c^{(*)}$ systems. The unit of the cutoff Λ is GeV. "…" means no such states at the S-wave level.

	$D\Sigma_c$		$D\Sigma_c^*$		$D^*\Sigma_c$		$D^*\Sigma_c^*$	
J^P	Λ	θ	Λ	θ	Λ	θ	Λ	θ
$\frac{1}{2}^-$	1.18	17.2°	…	…	1.18	17.4°	1.12	20.3°
	1.25	7.2°			1.22	7.6°	1.16	9.3°
	1.30	4.7°			1.25	4.6°	1.19	5.5°
$\frac{3}{2}^-$	…	…	1.18	17.1°	0.93	17.9°	1.08	19.5°
			1.25	7.3°	1.00	4.8°	1.14	6.3°
			1.30	4.8°	1.04	3.0°	1.18	3.7°
$\frac{5}{2}^-$	…	…	…	…	…	…	0.88	16.2°
							0.95	4.9°
							1.00	2.9°

$$\theta = \frac{180^\circ}{\pi}\arccos(\sqrt{P_{I=1/2}}), \tag{52}$$

with $P_{I=1/2}$ the probability of the isospin-1/2 state found in the mixed state. When $\theta = 0°$ (90°), the state is purely isospin-1/2 (3/2), corresponding to $P_{I=1/2} = 100\%$ ($P_{I=3/2} = 100\%$). In contrast, $\theta = 45°$ represents maximal isospin mixing, where the state has equal probability of being isospin-1/2 and isospin-3/2. In Table X, we present the numerical results of the isospin-breaking angle θ of the $D^{(*)}\Sigma_c^{(*)}$ systems.

Our results show that the isospin mixing angle lies approximately in the range $\theta = 3°$-20°. Notably, θ increases as the binding energy decreases: the more weakly bound the system, the larger the mixing angle. This implies that for hadronic molecular states, which are typically characterized by small binding energies, isospin-breaking effects are amplified. Such effects must therefore be incorporated in high-precision calculations to match the demands of rapidly developing experiments.

IV. CONCLUSION

In this work, we investigate the role of explicit isospin breaking in deuteronlike molecular states of the $D^{(*)}\Sigma_c^{(*)}$ systems within the framework of the OBE model. The isospin-breaking effects considered include the Coulomb interaction between charged hadrons, the threshold differences among components within the same isospin multiplet, and the mass splittings between charged and neutral exchanged light mesons—specifically, the pseudoscalar mesons $\pi^\pm$ and π^0, as well as the vector mesons $\rho^\pm$ and ρ^0.

Our results show that all four $D^{(*)}\Sigma_c^{(*)}$ systems with isospin $I = 1/2$ form well-bound states, with binding energies of several MeV for physically reasonable cutoff values. In contrast, for the isospin-3/2 configurations, the contributions from ρ and ω exchange largely cancel each other, resulting in a weak net interaction. Consequently, only the $D^*\Sigma_c$ and $D^*\Sigma_c^*$ systems with $J^P = 1/2^-$ are able to form weakly bound states within the reasonable momentum cutoff values. For these molecular candidates, we have explicitly included isospin-breaking effects: the Coulomb interaction between charged constituents, threshold differences among the $D^{(*)}\Sigma_c^{(*)}$ components within the same isospin multiplet, and the mass splittings between charged and neutral pions and ρ mesons in the exchange potentials. Owing to the shallow nature of the bound states, isospin breaking is found to induce a correction of 10%–30% to the binding energy. This sizable effect underscores the necessity of incorporating isospin breaking in high-precision theoretical calculations aimed at keeping pace with rapid experimental progress.

We also compute the mixing angle between different isospin states, i.e., $I = 1/2$ and $I = 3/2$ configurations, since the total isospin I is no longer conserved while its third component I_3 remains a good quantum number. We find that for very loosely bound states with small binding energies, this mixing angle can reach values as large as 18°–20°. However, the mixing angle rapidly decreases as the binding energy increases by finely tuning the momentum cutoff.

As experimental data on exotic hadronic states continue to accumulate, high-precision theoretical calculations that incorporate isospin-breaking effects are urgently needed. We hope that the present study of isospin breaking in hadronic molecular states will provide valuable guidance for future experimental searches for deuteronlike hadron molecules.

ACKNOWLEDGMENTS

This work is supported by the Special Funds for Theoretical Physics under the National Natural Science Foundation of China (Grant No. 12547105), the National Natural Science Foundation of China (Grant No. 12575153).

DATA AVAILABILITY

The data that support the findings of this study are openly available [69].

APPENDIX A: DETAILS OF OBE POTENIAL MODEL

1. The meson fields

In the OBE potential model, some of physical variables can be simplified. Expanding $\hat{\xi}^\mu$ in the axial and vector currents up to leading order, we obtain

$$\hat{\xi} \sim 1 + \mathrm{i}\mathbb{P}/f_\pi, \qquad \hat{\xi}^\dagger \sim 1 - \mathrm{i}\mathbb{P}/f_\pi, \tag{A1}$$

$$\hat{X}^\rho \sim \mathrm{i}\partial^\rho\mathbb{P}/f_\pi, \qquad \hat{V}^\rho \sim \mathbb{P}\partial^\rho\mathbb{P}/f_\pi^2, \tag{A2}$$

from which it is clear that there is no contribution from $\hat{V}^{\rho}$ at leading order. Similarly, for $\hat{F}^{\alpha\beta}$ we can omit the two-boson-exchange term $[\mathbb{V}'^{\alpha}, \mathbb{V}'^{\beta}]$, but keep $\hat{F}^{\alpha\beta} = \partial^{\alpha}\mathbb{V}'^{\beta} - \partial^{\beta}\mathbb{V}'^{\alpha}$.

2. The spin current operators

The Feynman rules of OBE potential model are

$$\begin{cases} \langle 0|\mathrm{M}|M\rangle \equiv \sqrt{m_{[M]}}, \\ \langle M|\mathrm{M}|0\rangle \equiv \sqrt{m_{[M]}}, \end{cases} \tag{A3}$$

$$\begin{cases} \langle 0|\mathrm{M}^{*\mu}|M^{*}\rangle \equiv \sqrt{m_{[M^{*}]}}\varepsilon^{\mu}(\lambda), \\ \langle M^{*}|\mathrm{M}^{*\mu}|0\rangle \equiv \sqrt{m_{[M^{*}]}}\bar{\varepsilon}^{\mu}(\lambda), \end{cases} \tag{A4}$$

$$\begin{cases} \langle 0|\mathrm{B}|\mathcal{B}\rangle \equiv \sqrt{2m_{[\mathcal{B}]}}u_{\mathrm{B}}(p,s), \\ \langle \mathcal{B}|\mathrm{B}|0\rangle \equiv \sqrt{2m_{[\mathcal{B}]}}\bar{u}_{\mathrm{B}}(p,s), \end{cases} \tag{A5}$$

$$\begin{cases} \langle 0|\mathrm{B}^{*\mu}|\mathcal{B}^{*}\rangle \equiv \sqrt{2m_{[\mathcal{B}^{*}]}}U^{\mu}_{\mathrm{B}^{*}}(p,m_j), \\ \langle \mathcal{B}^{*}|\mathrm{B}^{*\mu}|0\rangle \equiv \sqrt{2m_{[\mathcal{B}^{*}]}}\bar{U}^{\mu}_{\mathrm{B}^{*}}(p,m_j), \end{cases} \tag{A6}$$

where the polarization vectors, spinors and vector-spinors are defined, respectively, as follows:

$$\epsilon^{\mu}(+,0,-) \equiv \frac{1}{\sqrt{2}}\begin{bmatrix} 0 \\ -1 \\ -\mathrm{i} \\ 0 \end{bmatrix}, \quad \begin{bmatrix} 0 \\ 0 \\ 0 \\ 1 \end{bmatrix}, \quad \frac{1}{\sqrt{2}}\begin{bmatrix} 0 \\ 1 \\ -\mathrm{i} \\ 0 \end{bmatrix}, \tag{A7}$$

$$u_{\mathrm{B}}(p,s) = \sqrt{\frac{E_{\mathrm{B}}+m_{\mathrm{B}}}{2m_{\mathrm{B}}}}\begin{pmatrix} \chi_s \\ \frac{\vec{\sigma}\cdot\vec{p}}{E_{\mathrm{B}}+m_{\mathrm{B}}}\chi_s \end{pmatrix},$$

$$\bar{u}_{\mathrm{B}}(p',s') = \sqrt{\frac{E'_{\mathrm{B}}+m_{\mathrm{B}}}{2m_{\mathrm{B}}}}\left(\chi^{\dagger}_{s'}, \quad \frac{\vec{\sigma}\cdot\vec{p}'}{E'_{\mathrm{B}}+m_{\mathrm{B}}}\chi^{\dagger}_{s'}\right), \tag{A8}$$

$$U^{\mu}_{\mathrm{B}^{*}}(\vec{p},\phi) = \begin{pmatrix} \chi^{\mu}(\phi) \\ \frac{\vec{\sigma}\cdot\vec{p}}{2m_{\mathrm{B}^{*}}}\chi^{\mu}(\phi) \end{pmatrix},$$

$$\bar{U}^{\mu}_{\mathrm{B}^{*}}(\vec{p}',\phi') = \left(\chi^{\dagger\mu}(\phi'), \quad \frac{\vec{\sigma}\cdot\vec{p}'}{2m_{\mathrm{B}^{*}}}\chi^{\dagger\mu}(\phi')\right). \tag{A9}$$

The single spinors and single vector-spinors read, respectively, as

$$\chi_{1/2} = \begin{pmatrix} 1 \\ 0 \end{pmatrix}, \qquad \chi_{-1/2} = \begin{pmatrix} 0 \\ 1 \end{pmatrix}, \tag{A10}$$

$$\chi^{\mu}(\phi) \equiv \sum_{m_1,m_2} \mathrm{CG}\left[1m_1, \frac{1}{2}m_2, \frac{3}{2}\phi\right]\epsilon^{\mu}(m_1)\chi(m_2), \tag{A11}$$

along with CG[…] representing the Clebsch-Gordan coefficient.

In addition, we also introduce some simplified notation, which absorbs the mass parameters in the normalization into the Breit's formula,

$$V(\mathbf{q}) = -\mathcal{M}(12 \to 34), \tag{A12}$$

with

$$\langle 0|\mathrm{M}|M\rangle = 1/\sqrt{2}, \qquad \langle 0|\mathrm{M}^{*\mu}|M^{*}\rangle = \varepsilon^{\mu}_{\lambda}/\sqrt{2},$$
$$\langle M|\mathrm{M}|0\rangle = 1/\sqrt{2}, \qquad \langle M^{*}|\mathrm{M}^{*\mu}|0\rangle = \bar{\varepsilon}^{\mu}_{\lambda}/\sqrt{2}, \tag{A13}$$

$$\langle 0|\mathrm{B}|\mathcal{B}\rangle = u_{\mathrm{B}}, \qquad \langle 0|\mathrm{B}^{*\mu}|\mathcal{B}^{*}\rangle = U^{\mu}_{\mathrm{B}^{*}},$$
$$\langle \mathcal{B}|\mathrm{B}|0\rangle = \bar{u}_{\mathrm{B}}, \qquad \langle \mathcal{B}^{*}|\mathrm{B}^{*\mu}|0\rangle = \bar{U}^{\mu}_{\mathrm{B}^{*}}. \tag{A14}$$

3. The potentials in momentum space

Recalling the expression of n-pole form factor, we can rewrite its form as

$$F_n(\lambda,u,\mathbf{q}) = \left(\frac{\lambda^2-u^2}{\lambda^2+\mathbf{q}^2}\right)^n, \tag{A15}$$

$$\lambda^2 = \Lambda^2 - q_0^2, \qquad u^2 = m^2 - q_0^2. \tag{A16}$$

Separating the operators from the OBE potential for the heavy-flavor hadrons, we obtain three types of momentum currents,

$$V_0(\mathbf{q}) \sim \frac{1}{\mathbf{q}^2+u^2}, \qquad V_2(\mathbf{q}) \sim \frac{q^i q^j}{\mathbf{q}^2+u^2},$$
$$V_{\mathrm{S}}(\mathbf{q}) \sim \frac{\mathbf{q}^2}{\mathbf{q}^2+u^2} = \delta^{ij}\frac{q^i q^j}{\mathbf{q}^2+u^2}. \tag{A17}$$

In the above, $\mathbf{q}$ is the momentum of the exchanged light meson. Combining the monopole form factor $F_1(\lambda,u,\mathbf{q})$ and making the Fourier transform (taking away the general factor $1/4\pi$), we have

$$V_0(\mathbf{q}) \to V_0(r), \qquad V_{\mathrm{S}}(\mathbf{q}) \to V_{\mathrm{S}}(r),$$
$$V_2(\mathbf{q}) \to V_2(r) = \frac{1}{3}\delta^{ij}V_{\mathrm{S}}(r) + \frac{1}{3}\hat{T}^{ij}V_{\mathrm{T}}(r), \tag{A18}$$

where $\hat{T}^{ij} \equiv 3\hat{r}^i\hat{r}^j - \delta^{ij}$ and $\hat{r}$ is a unit direction vector. The basic functions can be written explicitly as

$$V_0(r) = uY(ur) - \lambda Y(\lambda r) - \kappa_0 e^{-\lambda r}, \tag{A19}$$

$$V_{\mathrm{S}}(r) = u^3Y(ur) - \lambda^3Y(\lambda r) - \kappa_2(\lambda r - 2)Y(\lambda r), \tag{A20}$$

$$V_{\mathrm{T}}(r) = u^3Y(ur)H(ur) - \lambda^3Y(\lambda r)H(\lambda r) - \kappa_2(\lambda r+1)Y(\lambda r), \tag{A21}$$

with some definitions,

$$Y(x) \equiv e^{-x}/x, \qquad H(x) \equiv 1 + 3/x + 3/x^2, \tag{A22}$$

$$\kappa_m \equiv \beta^2 \lambda^{m-1}/2, \qquad \beta^2 \equiv \lambda^2 - u^2. \tag{A23}$$

In derivation of the effective potentials, we perform partial wave analysis to obtain the matrices with respect to different partial waves. Then the potential can be written in the following form:

$$\mathcal{V}^J_{ab}(r,\Lambda,m) \equiv V_0(r)\mathbb{C}^J_{ab}, \tag{A24}$$

$$\mathcal{P}^J_{ab}(r,\Lambda,m) \equiv \frac{1}{3}V_{\rm S}(r)\mathbb{S}^J_{ab} + \frac{1}{3}V_{\rm T}(r)\mathbb{T}^J_{ab}, \tag{A25}$$

$$\mathcal{T}^J_{ab}(r,\Lambda,m) \equiv \frac{2}{3}V_{\rm S}(r)\mathbb{S}^J_{ab} - \frac{1}{3}V_{\rm T}(r)\mathbb{T}^J_{ab}, \tag{A26}$$

where $\mathbb{C},\mathbb{S},\mathbb{T}$ are spin matrices. J is the total angular momentum while a, b are indices of different systems, i.e., we use 11, 22, 33 and 44 to refer, respectively, to $D\Sigma_c, D\Sigma_c^*, D^*\Sigma_c$, and $D^*\Sigma_c^*$.

APPENDIX B: EXPLICIT EXPRESSIONS OF SPIN CURRENTS AND OBE POTENTIALS

The specific OBE potentials of $D^{(*)}\Sigma_c^{(*)}$ systems are

$$V_{11} = \frac{1}{4\pi}\left(-G_{\rm S}V^{\rm S}_{11} + \frac{1}{2}G_{\rm V}V^{\rm V}_{11}\right), \tag{B1}$$

$$V_{22} = \frac{1}{4\pi}\left(-G_{\rm S}V^{\rm S}_{22} + \frac{1}{2}G_{\rm V}V^{\rm V}_{22}\right), \tag{B2}$$

$$V_{33} = \frac{1}{4\pi}\left[\left(-G_{\rm S}V^{\rm S}_{33} + \frac{1}{2}G_{\rm V}V^{\rm V}_{33}\right) - \left(G_{\rm P}V^{\rm P}_{33} + \frac{2}{3}G_{\rm T}V^{\rm T}_{33}\right)\right], \tag{B3}$$

$$V_{44} = \frac{1}{4\pi}\left[\left(-G_{\rm S}V^{\rm S}_{44} + \frac{1}{2}G_{\rm V}V^{\rm V}_{44}\right) - \frac{3}{2}\left(G_{\rm P}V^{\rm P}_{44} + \frac{2}{3}G_{\rm T}V^{\rm T}_{44}\right)\right], \tag{B4}$$

in which the products of coupling constants are

$$G_{\rm S} = g_{\rm S} l_{\rm S}, \qquad G_{\rm V} = \beta\beta_{\rm S} g_{\rm V}^2,$$
$$G_{\rm P} = g g_1/f_\pi^2, \qquad G_{\rm T} = \lambda\lambda_{\rm S} g_{\rm V}^2. \tag{B5}$$

For each type, there exist

$$V^{\rm S}_{ab} \equiv \mathcal{V}^J_{ab}(m_\sigma), \tag{B6}$$

$$V^{\rm V}_{ab} \equiv \frac{1}{2}\mathcal{V}^J_{ab}(m_\omega) + \mathcal{I}\cdot\mathcal{V}^J_{ab}(m_\rho), \tag{B7}$$

$$V^{\rm P}_{ab} \equiv \frac{1}{6}\mathcal{P}^J_{ab}(m_\pi) + \mathcal{I}\cdot\mathcal{P}^J_{ab}(m_\eta), \tag{B8}$$

$$V^{\rm T}_{ab} \equiv \frac{1}{2}\mathcal{T}^J_{ab}(m_\omega) + \mathcal{I}\cdot\mathcal{T}^J_{ab}(m_\rho), \tag{B9}$$

where $\mathcal{I}$ is the isospin factor which are

TABLE XI. Nontrivial spin matrices of $D^{(*)}\Sigma_c^{(*)}$ systems with $J = \frac{1}{2},\frac{3}{2},\frac{5}{2}$. "×" means no such matrices at the leading order.

	$J^P = \frac{1}{2}^-$	$J^P = \frac{3}{2}^-$	$J^P = \frac{5}{2}^-$
$\mathbb{S}_{33}$	$\begin{pmatrix} 2 & \\ & -1 \end{pmatrix}$	$\begin{pmatrix} -1 & & \\ & 2 & \\ & & -1 \end{pmatrix}$	×
$\mathbb{T}_{33}$	$\begin{pmatrix} & \sqrt{2} \\ \sqrt{2} & 2 \end{pmatrix}$	$\begin{pmatrix} & -1 & -2 \\ -1 & & 1 \\ -2 & 1 & \end{pmatrix}$	×
$\mathbb{S}_{44}$	$\begin{pmatrix} \frac{5}{3} & & \\ & \frac{2}{3} & \\ & & -1 \end{pmatrix}$	$\begin{pmatrix} \frac{2}{3} & & & \\ & \frac{5}{3} & & \\ & & \frac{2}{3} & \\ & & & -1 \end{pmatrix}$	$\begin{pmatrix} -1 & & & \\ & \frac{5}{3} & & \\ & & \frac{2}{3} & \\ & & & -1 \end{pmatrix}$
$\mathbb{T}_{44}$	$\begin{pmatrix} 0 & \frac{-7}{\sqrt{45}} & \frac{2}{\sqrt{5}} \\ \frac{-7}{\sqrt{45}} & \frac{16}{15} & -\frac{1}{5} \\ \frac{2}{\sqrt{5}} & -\frac{1}{5} & \frac{8}{5} \end{pmatrix}$	$\begin{pmatrix} 0 & \frac{7}{\sqrt{90}} & -\frac{16}{15} & \frac{-\sqrt{14}}{10} \\ \frac{7}{\sqrt{90}} & 0 & \frac{-7}{\sqrt{90}} & \frac{-2}{\sqrt{35}} \\ -\frac{16}{15} & \frac{-7}{\sqrt{90}} & 0 & \frac{-1}{\sqrt{14}} \\ \frac{-\sqrt{14}}{10} & \frac{-2}{\sqrt{35}} & \frac{-1}{\sqrt{14}} & \frac{4}{7} \end{pmatrix}$	$\begin{pmatrix} 0 & \frac{2}{\sqrt{15}} & \frac{\sqrt{21}}{15} & \frac{-2\sqrt{14}}{5} \\ \frac{2}{\sqrt{15}} & 0 & \frac{\sqrt{35}}{15} & -\sqrt{\frac{32}{105}} \\ \frac{\sqrt{21}}{15} & \frac{\sqrt{35}}{15} & -\frac{16}{21} & \frac{-\sqrt{6}}{21} \\ \frac{-2\sqrt{14}}{5} & -\sqrt{\frac{32}{105}} & \frac{-\sqrt{6}}{21} & -\frac{4}{7} \end{pmatrix}$

$$\mathcal{I} = \begin{cases} 1, & I_{ab} = 1/2, \\ -1/2, & I_{ab} = 3/2, \end{cases} \tag{B10}$$

and $\mathcal{V}^J_{ab}, \mathcal{P}^J_{ab}, \mathcal{T}^J_{ab}$ are defined as Eqs. (A24), (A25), and (A26).

The spin currents for the $D^{(*)}\Sigma_c^{(*)}$ systems can be written as

$$\hat{\mathbb{C}}_{11} = \hat{\mathcal{C}}(1, \chi_4^\dagger \chi_2), \qquad \hat{\mathbb{C}}_{22} = \hat{\mathcal{C}}(1, \vec{\chi}_4^\dagger \cdot \vec{\chi}_2),$$
$$\hat{\mathbb{C}}_{33} = \hat{\mathcal{C}}(\vec{\epsilon}_3^* \cdot \vec{\epsilon}_1, \chi_4^\dagger \chi_2), \qquad \hat{\mathbb{C}}_{44} = \hat{\mathcal{C}}(\vec{\epsilon}_3^* \cdot \vec{\epsilon}_1, \vec{\chi}_4^\dagger \cdot \vec{\chi}_2), \tag{B11}$$

$$\hat{\mathbb{S}}_{33} = \hat{\mathcal{S}}(\mathrm{i}\vec{\epsilon}_3^* \times \vec{\epsilon}_1, \chi_4^\dagger \vec{\sigma} \chi_2),$$
$$\hat{\mathbb{S}}_{44} = \hat{\mathcal{S}}(\mathrm{i}\vec{\epsilon}_3^* \times \vec{\epsilon}_1, -\mathrm{i}\vec{\chi}_4^\dagger \times \vec{\chi}_2), \tag{B12}$$

$$\hat{\mathbb{T}}_{33} = \hat{\mathcal{T}}(\mathrm{i}\vec{\epsilon}_3^* \times \vec{\epsilon}_1, \chi_4^\dagger \vec{\sigma} \chi_2),$$
$$\hat{\mathbb{T}}_{44} = \hat{\mathcal{T}}(\mathrm{i}\vec{\epsilon}_3^* \times \vec{\epsilon}_1, -\mathrm{i}\vec{\chi}_4^\dagger \times \vec{\chi}_2), \tag{B13}$$

where

$$\hat{\mathcal{C}}(A, B) \equiv AB, \qquad \hat{\mathcal{S}}(\vec{A}, \vec{B}) \equiv \vec{A} \cdot \vec{B},$$
$$\hat{\mathcal{T}}(\vec{A}, \vec{B}) \equiv 3(\vec{A} \cdot \vec{r})(\vec{B} \cdot \vec{r}) - \vec{A} \cdot \vec{B}. \tag{B14}$$

One obtains the final matrix elements by projecting on the specific initial and final spin states

$$\mathbb{O}_{ab} = \langle L'S'J'm' | \hat{\mathbb{O}}_{ab} | LSJm \rangle. \tag{B15}$$

The nontrivial matrices $\mathbb{S}_{ab}$ and $\mathbb{T}_{ab}$ are listed in Table XI, while all of the $\mathbb{C}_{ab}$ matrices are just identity matrices.

[1] S. K. Choi *et al.* (Belle Collaboration), Observation of a narrow charmonium-like state in exclusive $B^\pm \to K^\pm \pi^+ \pi^- J/\psi$ decays, Phys. Rev. Lett. **91**, 262001 (2003).

[2] M. Ablikim *et al.* (BESIII Collaboration), Observation of a charged charmoniumlike structure in $e^+e^- \to \pi^+\pi^- J/\psi$ at $\sqrt{s} = 4.26$ GeV, Phys. Rev. Lett. **110**, 252001 (2013).

[3] Z. Q. Liu *et al.* (Belle Collaboration), Study of $e^+e^- \to \pi^+\pi^- J/\psi$ and observation of a charged charmoniumlike state at Belle, Phys. Rev. Lett. **110**, 252002 (2013); **111**, 019901(E) (2013).

[4] R. Aaij *et al.* (LHCb Collaboration), Observation of $J/\psi p$ resonances consistent with pentaquark states in $\Lambda_b^0 \to J/\psi K^- p$ decays, Phys. Rev. Lett. **115**, 072001 (2015).

[5] R. Aaij *et al.* (LHCb Collaboration), Observation of a narrow pentaquark state, $P_c(4312)^+$, and of two-peak structure of the $P_c(4450)^+$, Phys. Rev. Lett. **122**, 222001 (2019).

[6] R. Aaij *et al.* (LHCb Collaboration), Evidence of a $J/\psi\Lambda$ structure and observation of excited Ξ^- states in the $\Xi_b^- \to J/\psi\Lambda K^-$ decay, Sci. Bull. **66**, 1278 (2021).

[7] R. Aaij *et al.* (LHCb Collaboration), Observation of a $J/\psi\Lambda$ resonance consistent with a strange pentaquark candidate in $B^- \to J/\psi\Lambda p^-$ decays, Phys. Rev. Lett. **131**, 031901 (2023).

[8] R. Aaij *et al.* (LHCb Collaboration), Observation of an exotic narrow doubly charmed tetraquark, Nat. Phys. **18**, 751 (2022).

[9] E. S. Swanson, The new heavy mesons: A status report, Phys. Rep. **429**, 243 (2006).

[10] H.-X. Chen, W. Chen, X. Liu, and S.-L. Zhu, The hidden-charm pentaquark and tetraquark states, Phys. Rep. **639**, 1 (2016).

[11] H.-X. Chen, W. Chen, X. Liu, Y.-R. Liu, and S.-L. Zhu, A review of the open charm and open bottom systems, Rep. Prog. Phys. **80**, 076201 (2017).

[12] A. Hosaka, T. Iijima, K. Miyabayashi, Y. Sakai, and S. Yasui, Exotic hadrons with heavy flavors: X, Y, Z, and related states, Prog. Theor. Exp. Phys. **2016**, 062C01 (2016).

[13] A. Esposito, A. Pilloni, and A. D. Polosa, Multiquark resonances, Phys. Rep. **668**, 1 (2017).

[14] S. L. Olsen, T. Skwarnicki, and D. Zieminska, Nonstandard heavy mesons and baryons: Experimental evidence, Rev. Mod. Phys. **90**, 015003 (2018).

[15] N. Brambilla, S. Eidelman, C. Hanhart, A. Nefediev, C.-P. Shen, C. E. Thomas, A. Vairo, and C.-Z. Yuan, The *XYZ* states: Experimental and theoretical status and perspectives, Phys. Rep. **873**, 1 (2020).

[16] Y.-R. Liu, H.-X. Chen, W. Chen, X. Liu, and S.-L. Zhu, Pentaquark and tetraquark states, Prog. Part. Nucl. Phys. **107**, 237 (2019).

[17] H.-X. Chen, W. Chen, X. Liu, and X.-H. Liu, Establishing the first hidden-charm pentaquark with strangeness, Eur. Phys. J. C **81**, 409 (2021).

[18] H.-X. Chen, W. Chen, X. Liu, Y.-R. Liu, and S.-L. Zhu, An updated review of the new hadron states, Rep. Prog. Phys. **86**, 026201 (2023).

[19] LHCb Collaboration, Exotic hadron naming convention, arXiv:2206.15233.

[20] Z.-C. Yang, Z.-F. Sun, J. He, X. Liu, and S.-L. Zhu, The possible hidden-charm molecular baryons composed of anti-charmed meson and charmed baryon, Chin. Phys. C **36**, 6 (2012).

[21] J.-J. Wu, R. Molina, E. Oset, and B. S. Zou, Prediction of narrow N^* and Λ^* resonances with hidden charm above 4 GeV, Phys. Rev. Lett. **105**, 232001 (2010).

[22] M. Karliner and J. L. Rosner, New exotic meson and baryon resonances from doubly-heavy hadronic molecules, Phys. Rev. Lett. **115**, 122001 (2015).

[23] W. L. Wang, F. Huang, Z. Y. Zhang, and B. S. Zou, $\Sigma_c \bar{D}$ and $\Lambda_c \bar{D}$ states in a chiral quark model, Phys. Rev. C **84**, 015203 (2011).

[24] X.-Q. Li and X. Liu, A possible global group structure for exotic states, Eur. Phys. J. C **74**, 3198 (2014).
[25] J.-J. Wu, R. Molina, E. Oset, and B. S. Zou, Dynamically generated N^* and Λ^* resonances in the hidden charm sector around 4.3 GeV, Phys. Rev. C **84**, 015202 (2011).
[26] R. Chen, X. Liu, X.-Q. Li, and S.-L. Zhu, Identifying exotic hidden-charm pentaquarks, Phys. Rev. Lett. **115**, 132002 (2015).
[27] H.-X. Chen, W. Chen, X. Liu, T. G. Steele, and S.-L. Zhu, Towards exotic hidden-charm pentaquarks in QCD, Phys. Rev. Lett. **115**, 172001 (2015).
[28] R. Chen, J. He, and X. Liu, Possible strange hidden-charm pentaquarks from and interactions, Chin. Phys. C **41**, 103105 (2017).
[29] R. Chen, Z.-F. Sun, X. Liu, and S.-L. Zhu, Strong LHCb evidence supporting the existence of the hidden-charm molecular pentaquarks, Phys. Rev. D **100**, 011502 (2019).
[30] H.-X. Chen, E.-L. Cui, W. Chen, X. Liu, T. G. Steele, and S.-L. Zhu, QCD sum rule study of hidden-charm pentaquarks, Eur. Phys. J. C **76**, 572 (2016).
[31] R. Chen, A. Hosaka, and X. Liu, Heavy molecules and one-σ/ω-exchange model, Phys. Rev. D **96**, 116012 (2017).
[32] Y. Shimizu and M. Harada, Hidden charm pentaquark $P_c(4380)$ and doubly charmed baryon $\Xi^*_{cc}(4380)$ as hadronic molecule states, Phys. Rev. D **96**, 094012 (2017).
[33] R. Chen, N. Li, Z.-F. Sun, X. Liu, and S.-L. Zhu, Doubly charmed molecular pentaquarks, Phys. Lett. B **822**, 136693 (2021).
[34] X.-K. Dong, F.-K. Guo, and B.-S. Zou, A survey of heavy–heavy hadronic molecules, Commun. Theor. Phys. **73**, 125201 (2021).
[35] Z.-G. Wang, Analysis of the doubly heavy baryon states and pentaquark states with QCD sum rules, Eur. Phys. J. C **78**, 826 (2018).
[36] X.-W. Wang and Z.-G. Wang, Doubly-charm and doubly-bottom pentaquark molecular states via the QCD sum rules, Int. J. Mod. Phys. A **39**, 2450067 (2024).
[37] F.-B. Duan, Q.-N. Wang, Z.-Y. Yang, X.-L. Chen, and W. Chen, Doubly charmed pentaquark states in QCD sum rules, Phys. Rev. D **109**, 094018 (2024).
[38] Z.-Y. Yang, Q. Wang, and W. Chen, Mass spectra of strange double charm pentaquarks with strangeness $S = -1$, Phys. Rev. D **110**, 056022 (2024).
[39] Z.-Y. Yang and W. Chen, Decay and production properties of a strange double-charm pentaquark, Phys. Rev. D **113**, 054021 (2026).
[40] W. Chen, F.-B. Duan, Z.-Y. Yang, Q.-N. Wang, X.-L. Chen, and Q. Wang, Doubly charmed pentaquark states with strangeness $S = 0, -1$, Proc. Sci., QCHSC24 (**2025**) 127 [arXiv:2509.01965].
[41] Z.-H. Guo, Prediction of exotic doubly charmed baryons within chiral effective field theory, Phys. Rev. D **96**, 074004 (2017).
[42] K. Chen, B. Wang, and S.-L. Zhu, Exploration of the doubly charmed molecular pentaquarks, Phys. Rev. D **103**, 116017 (2021).
[43] L. Meng, B. Wang, G.-J. Wang, and S.-L. Zhu, Chiral perturbation theory for heavy hadrons and chiral effective field theory for heavy hadronic molecules, Phys. Rep. **1019**, 1 (2023).
[44] Q.-S. Zhou, K. Chen, X. Liu, Y.-R. Liu, and S.-L. Zhu, Surveying exotic pentaquarks with the typical $QQqq\bar{q}$ configuration, Phys. Rev. C **98**, 045204 (2018).
[45] G. Yang, J. Ping, and J. Segovia, Doubly charmed pentaquarks, Phys. Rev. D **101**, 074030 (2020).
[46] Y. Xing and Y. Niu, The study of doubly charmed pentaquark $cc\bar{q}qq$ with the SU(3) symmetry, Eur. Phys. J. C **81**, 978 (2021).
[47] S.-Y. Li, Y.-R. Liu, C.-R. Shu, and Z.-G. Si, Doubly-charmed pentaquark states in a mass splitting model, Eur. Phys. J. Plus **140**, 783 (2025).
[48] H.-T. An and Y.-S. Li, Systematic investigation of the spectroscopy and decay behaviors of doubly-charmed pentaquarks, arXiv:2512.08643.
[49] X. Liu, Y. Tan, X. Chen, D. Chen, H. Huang, and J. Ping, Investigation of the doubly charmed analog of the P_c states, Phys. Rev. C **113**, 015208 (2026).
[50] C.-W. Shen, Y.-h. Lin, and U.-G. Meißner, P^N_{cc} states in a unitarized coupled-channel approach, Eur. Phys. J. C **83**, 70 (2023).
[51] Y. Lyu, H. Tong, T. Sugiura, S. Aoki, T. Doi, T. Hatsuda, J. Meng, and T. Miyamoto, Dibaryon with highest charm number near unitarity from lattice QCD, Phys. Rev. Lett. **127**, 072003 (2021).
[52] M.-Z. Liu and L.-S. Geng, Prediction of an $\Omega_{bbb}\Omega_{bbb}$ dibaryon in the extended one-boson exchange model, Chin. Phys. Lett. **38**, 101201 (2021).
[53] N. Mathur, M. Padmanath, and D. Chakraborty, Strongly bound dibaryon with maximal beauty flavor from lattice QCD, Phys. Rev. Lett. **130**, 111901 (2023).
[54] P. Chen, Z.-W. Liu, Z.-L. Zhang, S.-Q. Luo, F.-L. Wang, J.-Z. Wang, and X. Liu, Role of electromagnetic interactions in the $X(3872)$ and its analogs, Phys. Rev. D **109**, 094002 (2024).
[55] N. Li and S.-L. Zhu, Isospin breaking, coupled-channel effects, and $X(3872)$, Phys. Rev. D **86**, 074022 (2012).
[56] T.-M. Yan, H.-Y. Cheng, C.-Y. Cheung, G.-L. Lin, Y. C. Lin, and H.-L. Yu, Heavy quark symmetry and chiral dynamics, Phys. Rev. D **46**, 1148 (1992); **55**, 5851(E) (1997).
[57] M. B. Wise, Chiral perturbation theory for hadrons containing a heavy quark, Phys. Rev. D **45**, R2188 (1992).
[58] G. Burdman and J. F. Donoghue, Union of chiral and heavy quark symmetries, Phys. Lett. B **280**, 287 (1992).
[59] R. Casalbuoni, A. Deandrea, N. Di Bartolomeo, R. Gatto, F. Feruglio, and G. Nardulli, Phenomenology of heavy meson chiral Lagrangians, Phys. Rep. **281**, 145 (1997).
[60] A. F. Falk and M. E. Luke, Strong decays of excited heavy mesons in chiral perturbation theory, Phys. Lett. B **292**, 119 (1992).
[61] Y.-R. Liu and M. Oka, $\Lambda_c N$ bound states revisited, Phys. Rev. D **85**, 014015 (2012).
[62] Y.-R. Liu, X. Liu, W.-Z. Deng, and S.-L. Zhu, Is $X(3872)$ really a molecular state?, Eur. Phys. J. C **56**, 63 (2008).
[63] X. Liu, Z.-G. Luo, Y.-R. Liu, and S.-L. Zhu, X(3872) and other possible heavy molecular states, Eur. Phys. J. C **61**, 411 (2009).

[64] R. Machleidt, K. Holinde, and C. Elster, The bonn meson exchange model for the nucleon nucleon interaction, Phys. Rep. **149**, 1 (1987).

[65] M. Goitein, J. R. Dunning, Jr., and R. Wilson, Comparison of elastic electron-proton scattering cross sections with some theoretical predictions, Phys. Rev. Lett. **18**, 1018 (1967).

[66] N. Auerbach, J. Hufner, A. K. Kerman, and C. M. Shakin, A theory of isobaric analog resonances, Rev. Mod. Phys. **44**, 48 (1972).

[67] K. U. Can, G. Erkol, B. Isildak, M. Oka, and T. T. Takahashi, Electromagnetic structure of charmed baryons, Proc. Sci., Hadron2013 (**2013**) 057.

[68] R. Chen, A. Hosaka, and X. Liu, Heavy molecules and one-σ/ω-exchange model, Phys. Rev. D **96**, 116012 (2017).

[69] F.-Y. Chen, N. Li, and W. Chen, Dataset for isospin-breaking effects of double charm molecular pentaquarks, 10.5281/zenodo.20727778 (2026).